COMPARISON OF INTERACTION OF POLY (ETHYLENE GLYCOL) AND POLY (OLIGO (ETHYLENE GLYCOL) METHYL ETHER METHACRYLATE) WITH WATER USING MOLECULAR DYNAMICS SIMULATION

A Thesis Submitted to
The Graduate School of Engineering and Sciences of
Izmir Institute of Technology
in Partial Fulfilment of the Requirements for the Degree of

MASTER OF SCIENCE

in Polymer Science and Engineering

by
Yawer ABBAS

March 2025
IZMIR

We approve the thesis of **Yawer ABBAS.**

Examining Committee Members:

_____

Prof. Dr. Volga BULMUŞ

Department of Bioengineering, Izmir Institute of Technology

_____

Assoc. Professor Dr. Beste BAYRAMOĞLU

Department of Food Engineering, Izmir Institute of Technology

_____

Assoc. Professor Dr. Ahmet AYKAÇ

Department of Engineering Sciences, Katip Çelebi University

13 March 2025

_____

Prof. Dr. Volga BULMUŞ

Supervisor, Department of Bioengineering,

Izmir Institute of Technology

_____

Assistant Prof. Dr. Arzu UYAR

Co-Supervisor, Department of Bioengineering, Izmir Institute of Technology

_____

Prof. Dr. Ekrem ÖZDEMIR

Head of the Polymer Science and Engineering Department

_____

Prof. Dr. Mehtap EANES

Dean of the Graduate School

ACKNOWLEDGEMENT

First and foremost, I express my deepest gratitude to Almighty Allah, whose grace and guidance have been my constant source of strength and perseverance throughout my academic journey abroad.

I am profoundly grateful to Professor Dr. Volga Bulmuş for her invaluable guidance, insightful suggestions, and steadfast support, which have greatly influenced the direction and success of this research. My heartfelt thanks also extend to my co-supervisor, Assistant Professor Dr. Arzu Uyar, for her constructive feedback, encouragement, and continuous support at every stage of this work. Their mentorship has been a cornerstone of my academic growth.

I wish to acknowledge the thoughtful contributions of my thesis committee members, Assoc. Professor Dr. Beste Bayramoğlu and Assoc. Professor Dr. Ahmet Ahmet Aykaç. Their insightful comments and expert advice have enriched this research and expanded my perspective for future academic pursuits.

A special thanks go to the Izmir Institute of Technology for fostering an exceptional academic and research environment. The institution's commitment to excellence and its supportive atmosphere for international students have provided me with invaluable learning opportunities and a strong sense of belonging.

I am eternally grateful to my family for their unwavering support, encouragement, and prayers throughout this challenging yet rewarding journey. Their steadfast belief in me has been a source of strength and inspiration.

Lastly, I would like to extend my sincere appreciation to my friends, both in Turkey and back home. Their unwavering encouragement, camaraderie, and kindness have been a constant source of motivation, making this experience all the more fulfilling.

I am profoundly thankful to everyone who has been a part of this journey.

ABSTRACT

COMPARISON OF INTERACTION OF POLY(ETHYLENE GLYCOL) AND POLY(OLIGO (ETHYLENE GLYCOL) METHYL ETHER METHACRYLATE) WITH WATER USING MOLECULAR DYNAMICS SIMULATION

This thesis compares the interaction of polyethylene glycol (PEG) and poly(oligo(ethylene glycol) methacrylate) (POEGMA) with water, by studying the conformational, hydration and H-bonding properties using MD simulations. Molecular models of POEGMA with 4-, 8-, 12-, 16- and 20 and PEG with 20- and 40 repeating units were prepared using Avogadro and CHARMM GUI software. All polymers were solvated in TIP3 water boxes. Charmmff parameters were used for the bonded and non-bonded interactions. The MD simulations were performed on TRUBA high-performance computing platform using LAMMPS software. After short minimization and 1 ns equilibration runs, 15 s of production run was carried out. The resulting trajectories were organized and analyzed using VMD software and MD analysis, and key properties like radius of gyration(Rg), watershell and hydrogen-bonding were investigated to compare the behaviour of two polymers in aqueous environment.

The results revealed distinct differences in both polymers. PEG exhibited Rg values which were slightly lower and less stable (9.73 and 13.41 Å of mean values for each PEG chains) conformations forming compact random helical structure, when compared with POEGMA having the same number of repeating ethylene glycol units. The watershell analysis showed that the number of water molecules (N(H2O)) in the watershell around PEG (mean N(H2O) of 244.9 and 418.6 for PEG20 and 40, respectively) is not stable mainly due to the unstable structure. Lastly, a higher average H-bond count is observed with PEG, when compared with POEGMA. On the other hand, POEGMA showed slightly higher Rg values but stable structure for shorter chains (13.46 and 15.78 Å for 4- and 8-mers POEGMA, respectively). The increase in Rg values with chain size was small compared to PEG. POEGMA chains also showed much more stable and more N(H2O). However, the H-bond counts for equivalent POEGMA were lower. The H-bond distribution along chain was also distinct for PEG and POEGMA chains.

Keywords: PEG, POEGMA, MD Simulation, Radius of gyration, watershell analysis, H-bond analysis

ÖZET

POLİ(ETİLEN GLİKOL) VE POLİ(OLİGO(ETİLEN GLİKOL) METİLETER METAKRİLAT) POLİMERLERİNİN SU İLE ETKİLEŞİMİNİN MOLEKÜLER DİNAMİK SİMÜLASYONU İLE KARŞILAŞTIRILMASI

Bu tez, MD simülasyonları kullanarak konformasyonel, hidrasyon ve H-bağlanma özelliklerini inceleyerek polietilen glikol (PEG) ve poli(oligo(etilen glikol) metakrilat) (POEGMA)'ın su ile etkileşimini karşılaştırmaktadır. 4, 8, 12, 16 ve 20 tekrarlayan birim içeren POEGMA ile 20 ve 40 birim içeren PEG'in moleküler modelleri Avogadro ve CHARMM GUI yazılımları kullanılarak hazırlanmıştır. Tüm polimerler TIP3 su kutularında çözündürülmüştür. Bağlanmış ve bağlanmamış etkileşimler için Charmmff parametreleri kullanıldı. MD simülasyonları TRUBA yüksek performanslı hesaplama platformunda LAMMPS yazılımı kullanılarak gerçekleştirilmiştir. Kısa minimizasyon ve 1 ns'lik dengeleme çalışmalarının ardından 15 s'lik üretim çalışması gerçekleştirilmiştir. Elde edilen yörüngeler VMD yazılımı ve MD analizi kullanılarak düzenlenmiş ve analiz edilmiştir. İki polimerin sulu ortamdaki davranışlarını karşılaştırmak için dönme yarıçapı (Rg), su kabuğu ve hidrojen bağı gibi temel özellikler araştırılmıştır.

Sonuçlar her iki polimerde de belirgin farklılıklar ortaya koymuştur. PEG, aynı sayıda tekrar eden etilen glikol birimine sahip POEGMA ile karşılaştırıldığında, kompakt rastgele sarmal yapı oluşturan biraz daha düşük ve daha az kararlı (her bir PEG zinciri için ortalama 9,73 ve 13,41 Å) Rg değerleri sergilemiştir. Su kabuğu analizi, PEG etrafındaki su kabuğundaki su molekülü sayısının (N(H2O)) (PEG20 ve 40 için sırasıyla ortalama N(H2O) 244.9 ve 418.6) esas olarak kararlı olmadığını göstermiştir. Su molekülü sayısındaki kararsızlık, konformasyonun kararsız olmasına atfedilmiştir. Son olarak, POEGMA ile karşılaştırıldığında, PEG ile daha yüksek bir ortalama H-bağı sayısı gözlemlenmiştir. Öte yandan, POEGMA biraz daha yüksek Rg değerleri ve kısa zincirler için kararlı bir yapı sergilemiştir (4 ve 8-mers POEGMA için sırasıyla 13,46 ve 15,78 Å). Zincir boyutu ile Rg değerlerindeki artış PEG'e kıyasla daha küçük çıkmıştır. Ayrıca, POEGMA zincirlerinin çok daha kararlı ve daha fazla N(H2O) değerlerine sahip olduğu bulunmuştur. Bununla birlikte, eşdeğer POEGMA için H-bağı sayılarının daha düşük

olduğu bulunmuştur. Zincir boyunca H-bağı dağılımı da PEG ve POEGMA zincirleri için farklıdır.

Anahtar Kelimeler: PEG, POEGMA, MD simulasyonu, dönme yarıçapı, su kabuğu analizi, H bağı analizi

Dedicated to my loving parents

TABLE OF CONTENTS

LIST OF FIGURES xi

LIST OF TABLES xiii

LIST OF ABBREVIATIONS xiv

CHAPTER 1 INTRODUCTION 1

1.1. POLYETHYLENE GLYCOL (PEG) 1

1.2. POLY (OLIGO (ETHYLENE GLYCOL) METHYL ETHER METHACRYLATE) (POEGMA) 4

1.3. MOLECULAR DYNAMICS SIMULATIONS 6

1.3.1. Brief History of MD 7

1.3.2. The Basic Algorithm of MD 8

1.4. FORCE FIELD 11

1.4.1. CHARMM Force Field 12

1.4.2. Bonded PE Terms 13

1.4.3. Non-Bonded Potentials 15

1.5. PROBLEM STATEMENT 17

CHAPTER 2 LITERATURE REVIEW 20

2.1. PEG 20

2.2. POEGMA 24

CHAPTER 3 COMPUTATIONAL METHODOLOGY and THEORY 30

3.1. MOLECULAR DESIGN AND CONFIGURATION 30

3.1.1. PEG 30

3.1.2. POEGMA 31

3.1.3. Simulation Parameters 32

3.2. LAMMPS 34

3.3. SIMULATION ANALYSIS 34

3.3.1. Radius of Gyration (Rg) 34

3.3.2. Watershell Analysis 35

3.3.3. Hydrogen-Bond Analysis 35

CHAPTER 4 RESULTS AND DISCUSSION 37
4.1. RADIUS OF GYRATION (RG) 37
4.2. WATERSHELL ANALYSIS 41
4.3. HYDROGEN BONDING ANALYSIS 43

CHAPTER 5 CONCLUSIONS and Recommendations 51
5.1. CONCLUSIONS 51
5.2. RECOMMENDATIONS AND FUTURE DIRECTIONS 52

REFERENCES 53

APPENDICES

Appendix A. GRAPHS OF RADIUS OF GYRATION ANALYSIS 61

Appendix B. GRAPHS OF WATERSHELL ANALYSIS 63

Appendix C. GRAPHS OF HYDROGEN BOND ANALYSIS 71

LIST OF FIGURES

Figure Page

Figure 1.1. The chemical formula of PEG 1

Figure 1.2. POEGMA Chemical Schematic 4

Figure 1.3. Bond Stretching and Associated Potential Energy Curve 13

Figure 1.4. Bond energy (E) as a function of bond angle (θ) with a three-atom schematic 14

Figure 1.5. Dihedral energy (E) as a function of torsion angle (τ) with a four-atom schematic. 15

Figure 1.6. Electrostatic potential with respect to r. 16

Figure 1.7. Lennard-Jones potential schematics 16

Figure 3.1. (a) PEG20 and (b) PEG40 in water box, (c) PEG20 and (d) PEG40 molecular model surrounded by water molecules. 31

Figure 3.2. (a) POEGMA4, (b) POEGMA8, (c) POEGMA12, (d) POEGMA16 and (e) POEGMA20 initial molecular model surrounded by water molecules 32

Figure 3.3. H-bond schematic showing the cutoff distance and angle 36

Figure 4.1. PEG20 and PEG40 Radius of Gyration. 38

Figure 4.2. R_g distribution box plot of PEG20 and PEG40 39

Figure 4.3. POEGMA -4, -8, -12, -16 and -20mers radius of gyration 40

Figure 4.4. PEG20 and PEG40 watershell analysis. 42

Figure 4.5. All POEGMA watershell analysis comparison 43

Figure 4.6. (Left) Both PEG mers Hbond count for each frame. (Right) PEG20, and 40 H-bond distribution for each Oxygen in the polymer 44

Figure 4.7. H-bond count for each frame for all POEGMA –mers. 45

Figure 4.8. Number of H-bonds for each oxygen atom for the whole simulation 46

Figure 4.9. H-bond count distribution for -4, -8, -12, -16 and -20mers POEGMA Oxygen atoms 48

Figure 4.10. PEG20 and PEG40 Rg analysis (top left), Watershell analysis (top right) and H-bond analysis (bottom) graphs. 49

Figure A.1. PEG20(left) and PEG40(Right) radius of gyration 61

Figure A.2. All POEGMA Rg distribution plot 62

Figure B.1. PEG20(left) and PEG40(right) watershell N(H2O) plot for each frame 64

Figure B.2. POEGMA -4, -8, -12, -16 and -20mers watershell N(H2O) 65

Figure B.3. POEGMA-4 snapshots at different stages of simulation run 66

Figure B.4. POEGMA-8 Snapshots at different stages of simulation run 67

Figure B.5. POEGMA-12 snapshots at different stages of simulation run 68

Figure B.6. POEGMA-16 Snapshots at different stages of simulation run 69

Figure B.7. POEGMA-20 snapshots at different stages of simulation run 70

Figure C.1. PEG20 and PEG40 H-bond count distribution for each frame 72

Figure C.2. POEGMA -4, -8, -12, -15 and -20mers H-bond count distribution 73

LIST OF TABLES

Table 1. Common thermodynamic ensemble employed in MD simulation. 10

LIST OF ABBREVIATIONS

PEG	Poly(Ethylene Glycol)
POEGMA	Poly(Ethylene Glycol Methyl Ether Methacrylate)
OEG	Oligo(Ethylene Glycol)
PEO	Poly(ethylene oxide)
MD	Molecular Dynamics
MC	Monte Carlo
LCST	Lower Critical Solution Temperature
UCST	Upper Critical Solution Temperature
NVE	Micro-canonical Ensemble
NVT	Canonical Ensemble
NPT	Isothermal-Isobaric Ensemble
NP	Nanoparticle
CHARMM	Chemistry at Harvard using Molecular Mechanics
AMBER	Assisted Model Building with Energy Refinement
OPLS	Optimized Parameters for Large-scale Simulations
GROMOS	Groningen Molecular Simulation
MMFF	Merck Molecular Force Field
GAFF	General AMBER Force Field
R_g	Radius of gyration
GROMACS	Groningen Machine for Chemical Simulations
LAMMPS	Large-scale Atomic/Molecular Massively Parallel Simulator
Mw	Molecular Weight
Wp	Weight fraction

Rh	Hydrodynamic radius
ATPS	Aqueous Two-Phase Systems
RDF	Radial Distribution Function
ATRP	Atom Transfer Radical Polymerization
DLS	Dynamic Light Scattering
SPR	Surface Plasmon Resonance
NR	Neutron Reflectometry
N(H2O)	Number of water molecules
AFM	Atomic Force Microscopy

CHAPTER 1

INTRODUCTION

The first chapter contains an overview of poly(ethylene glycol) (PEG), poly(oligo(ethylene glycol) methacrylate) (POEGMA), and Molecular Dynamics (MD) Simulation, along with the problem definition and the importance of the research.

1.1. Polyethylene glycol (PEG)

PEG is a linear or branched, neutral polyether, available in various molecular weights and soluble in water and most organic solvents. The chemical formula of PEG is presented in figure 1.1:

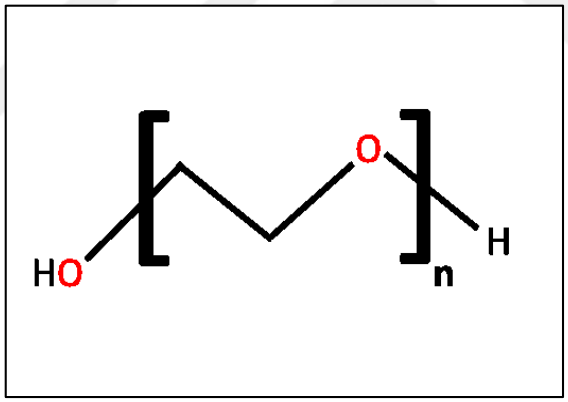

Figure 1.1 The chemical formula of PEG

PEGs are also sometimes called poly (ethylene oxide) (PEO); poly (ethylene glycol) refers to polyols of molecular weights below about 20,000, and poly (ethylene oxide) refers to higher molecular weight polymers. PEG has a strange solubility pattern, as it is soluble in water and many organic solvents; therefore, PEG is frequently described as amphiphilic.[1] Since PEG is soluble in both organic and aqueous media, it is apparent that the polymer will be present in both phases of an organic-water, two-phase system[2]. In biological systems, PEG partitions between aqueous medium and cell membranes, and

it induces cell fusion, which is used in the production of hybridomas and monoclonal antibodies.[3–5]

PEG solubility and partitioning patterns can be altered by attachment of hydrophobic tails or branches by including hydrophobic co-monomers in the polymer backbone, as in the typical ethylene oxide-propylene oxide copolymers, which can make it water-soluble if the latter's subunit is more than half of the total number.[1] This alteration in solubility can be used to control the partitioning of PEG derivatives in two-phase systems, such as benzene versus water, where attachment of hydrocarbon tails shifts partitioning in favor of the organic layer.[6]

PEGs also have the unusual property of possessing a lower critical solution temperature (LCST), or cloud point, of approximately 100°C in water; raising the temperature above 100°C will result in insolubility and formation of two phases.[7,8] The LCST for PEG varies somewhat depending on molecular weight, concentration, and pH. Increasing salt concentration can significantly lower the LCST. Also, including propylene oxide co-monomer lowers the LCST proportionately until the polymer with 60% ethylene oxide and 40% propylene oxide becomes insoluble at 37°C. The attachment of hydrophobic end groups has a similar effect, and this solubility-temperature relationship in water has several practical applications.[9]

Polyethylene glycol (PEG) is a highly versatile polymer extensively used in various scientific fields, particularly in drug delivery systems, because it is biocompatible and non-toxic.[10,11] PEG exhibits a remarkable ability to exclude other polymers in aqueous environments, which underlies its key properties, such as protein rejection, the formation of two-phase systems with other polymers, and its non-immunogenic and non-antigenic nature.[9] PEG is non-toxic and interacts with cell membranes without damaging active proteins or cells, enabling cell fusion, which is a critical part of biotechnology processes.[3–5] PEG's versatility is evident in its applications; its chemical structure allows for easy modification and attachment to other molecules and nanoparticles, which has minimal impact on their chemistry but significantly enhances solubility and increases molecular size, facilitating the separation of proteins and nucleic acids from solution for purification.[12–14] When mixed with a buffer, PEG forms aqueous polymer two-phase systems that are highly suitable for biological materials, making them highly effective for purification purposes.[2]

PEGylation, the covalent attachment of PEG chains to macromolecules or nanoparticles, improves solubility, stability[15], and biocompatibility, thereby improving pharmacokinetic and pharmacodynamics profiles, which ultimately increases the efficacy and safety of therapeutic agents.[10,16] PEGylation results in active conjugates that are non-immunogenic, non-antigenic and have significantly extended serum life.[16] PEGylation has demonstrated the ability to augment the therapeutic efficacy of several pharmaceuticals, encompassing small molecules such as proteins, peptides and nucleic acids.[17,18] PEG coating has multiple benefits in drug delivery systems, such as extended systemic circulation duration, safeguarding against degradation by enzymatic processes, increased cellular absorption, and enhanced targeted delivery.[11] Research has shown that the covalent binding of PEG to surfaces markedly diminishes protein adsorption.[19]

The stealth nature of PEG arises from its molecular and physical characteristics. The pronounced hydrophilic characteristics of PEG chains, when attached to proteins and nanoparticles, enable each PEG subunit to be enveloped by a minimum of 2-3 molecules of water.[20,21]As a result, this makes a water layer with a large excluded volume that prevents neighboring nanoparticles and/or blood components or proteins from penetrating the core and interacting with the core of PEGylated nanoparticle or molecule by electrostatic or hydrophobic interactions.[22–24] PEG is highly flexible and exhibits high chain mobility, leading to an extensive array of polymer chain conformations. Thus, any significant limitation of PEG's structural freedom, including the motion of its chains by arriving biological molecules, is thermodynamically unfavorable.[25,26] These features inhibit the interaction between the PEGylated nanoparticles and the biological environment. The amalgamation of these qualities renders PEG an essential instrument in biotechnology and medicine, especially in drug delivery systems.

Polyethylene glycol (PEG) is the most commonly used stealth polymer in skin care products, nutrition, and drug delivery, with many PEGylated products accessible on retail shelves and several others in clinical testing.[27] The over-exposure to products including PEG in various fields has led to the polymer losing its stealth characteristics, as scientists have observed immune response to PEGylated biomolecules. Many researchers have stated that the immunological response to PEG-conjugated drug molecules, caused rapid removal of the drugs from the system, losing their efficacy.[24,28,29] Moreover, similar scientific reports on fast clearance of the pegylated drug from human and animal blood circulation have held PEG-specific antibodies for the phenomenon, leading to its low

efficiency.[30–32] Furthermore, recent studies have also pointed out that anti-PEG antibodies could be present, even in those people who have never been administered any PEG-conjugated drugs in their lives.[33] Apart from the low effectiveness and rapid blood clearance, some clinical reports have observed such drugs triggering hypersensitivity and sometimes severe allergic responses in patients.[34] Recently there has been a push to discover and develop alternative non-fouling stealth polymers which can reduce the problems and limitations of PEG.[35]

1.2. Poly (Oligo (Ethylene Glycol) Methyl Ether Methacrylate) (POEGMA)

POEGMA (Poly (Oligo (ethylene glycol) methyl ether methacrylate)) has been investigated and garnered attention from various fields like biotechnology and the pharmaceutical industry. It has a branch or brush polymer structure comprising of its hydrophobic methyl methacrylate backbone and OEG (oligo (ethylene glycol)) side chains, which are hydrophilic in nature. The properties and beneficial characteristics of OEG have been detailed above. The chemical structure is presented in Figure 1.2:

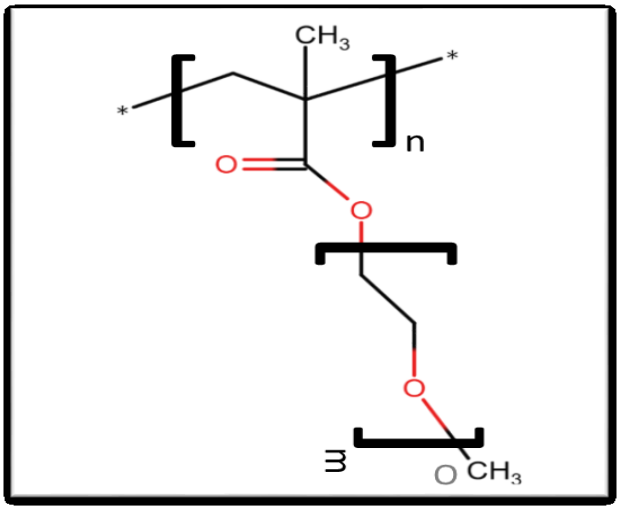

Figure 1.2 POEGMA Chemical Schematic

POEGMA's OEG branches have several useful chemical properties like non-toxic, non-immunogenic, and good biocompatibility which makes them extremely prized in the fields of biotechnology and medicine.[36,37] It is a thermos-responsive polymer, with its LCST highly dependent on the length of its OEG branches. The LCST of the polymer

according to needs can be tuned by simply altering the length OEG branches.[38–40] This property is vital in controlled drug delivery processes, because it enables accurate adjustment of the polymer solubility for different environmental temperatures. The extremely hydrophilic OEG branches create a steric wall that bars the conjugated nanoparticles' interactions with surrounding proteins. This low non-specific adsorption and non-fouling characteristics are extremely important in pharmaceutical industry as it increases the blood circulation half-life of the drugs, by reducing their detection and removal by the immune system, using their stealth properties.[16,41]

As a result, POEGMA has the ability to improve the pharmacokinetic properties of the conjugated nanoparticles. The coating of a molecule by POEGMA increases the dispersion of the in aqueous environments, improving the solubility and the diffusion of the drug molecule in the said media.[31,42,43] It can also be employed in modification of proteins, nanoparticle surfaces and nano-carriers. The attachment of POEGMA on these nano-carriers enhances their stability and antifouling characteristics, diminishes accumulation, and limits uptake by the reticuloendothelial system (RES), hence prolonging their blood circulation period within one's body.[44–47]

POEGMA can grafted onto the surfaces to develop surface coating, that repel proteins, which is of vital importance for biomedical engineering field, as the medical implants may be contaminated by the adsorption of proteins or the immune system recognition as a foreign substance leading to eventual failure of the devices. POEGMA conjugation on the surface of the device can improve biocompatibility of such devices and coatings have the potential to enhance the bio-compatibility of such devices and extend their usable lifespan[48]. Moreover, it can improve the sensitivity and reliability of biosensors by preventing non-specific protein adsorption to the monolayer surfaces.[41] Furthermore, the hyper branching of the polymer enables hydrogels based it to be effectively used as cell culture scaffold.[49] The biocompatibility of the polymer, along with its adjustable physical characteristics, renders it ideal for facilitating cell growth and differentiation.

Various controlled polymerization techniques such as RAFT and ATRP allowing great control of molecular weight and architecture can be utilized to synthesize POEGMA. This versatility and control of the molecular structure lets POEGMA to be tailored according to specific purposes.[41] The architecture as well as the molecular weight are pivotal in determining and tuning the properties like solubility viscosity and

hydrophilicity of POEGMA bases materials and their utility. In general, the hydrophilicity and blood clearance time increase with the increased molecular weight of the polymer. Sano et al.'s cellular uptake and blood circulation lifetime studies of POEGMA conjugated nanoparticles suggested that compared to PEG, POEGMA is potentially a better stealth polymer option.[50]

1.3. Molecular Dynamics Simulations

Computer simulation techniques have been devised to emulate the fluctuating responses of systems and are used frequently across several disciplines of science, especially in macromolecular complexes and the biological sciences. Two of the foremost widely used mathematical techniques include Monte Carlo (MC) and Molecular Dynamics (MD) simulations. Both approaches are effective instruments for investigating the behaviour of complex systems. However, they diverge markedly in their methodologies and capacities. The progress of these computational techniques can be traced to critical events in the history of science. MC simulations were first employed during the Manhattan Project in World War II to model nuclear detonation processes. Later, in the mid-1950s, Fermi, Tsingou, Pasta, and Ulam introduced Molecular Dynamics as an alternative technique, which models the behaviour of molecules in a system as they evolve over time, following Newton's laws of motion.[51] Although MC methods are successful, molecular dynamics simulations have become more prominent because they can simulate time-dependent molecule behaviors, providing a more comprehensive insight of system dynamics. MD simulations have developed into an important instrument to further research in molecular biology and macromolecular systems by detailing chronological progression and interactions among molecules.[52,53]

MC simulations are run by generating a collection of configurations and structures via arbitrary variations, prioritizing those with reduced total energy and elevated probability. This method is especially efficient for testing equilibrium conditions and evaluating the statistical characteristics of systems. Nonetheless, MC simulations cannot offer details into a system's time-based progression, hence constraining their applicability in investigations necessitating time-dependent analysis.[54]

On the other hand, MD simulations accurately simulate molecular behavior as it evolves by computing their locations and momenta according to Newton's equations of

motion. The chronological evolution of the structure, also known as a trajectory, facilitates comprehensive time-dependent analysis, encompassing rheological parameters, transport coefficients, spectra, and system reactions following disturbances. MD simulations are especially beneficial for examining interactions in bio-molecular systems, as they offer a detailed trajectory of molecular movements and include dynamic characteristics that MC simulations fail to represent.[53,54]

1.3.1. Brief History of MD

In the second half of the 1950s, molecular dynamics approaches first appeared in theoretical particle physics groups of researchers. The initial molecular dynamics simulations were performed by Alder and Wainwright in 1957, employing a hard-sphere model where atoms reacted solely by ideal collisions of elastic nature.[55] In 1964, Rahman created a seamless, continuous potential to mimic more accurate atomic interactions, expanding onward the previous approach.[56]

By the 1970s, major developments in computational science enabled the application of MD simulations to ever more sophisticated and massive systems, such as proteins, DNA, and macromolecules. This growth enabled the application of computer simulations in other disciplines, including materials science, biophysics, and biochemistry [57]. In 1971, Rahman and Stillinger performed the inaugural MD simulation of liquid water, subsequently conducting a simulation to examine the influence of temperature on water, and enhanced molecular dynamics in 1974.[58–60] In 1977, the earliest protein simulation focused on the bovine pancreatic trypsin inhibitor was a significant breakthrough in the field of computational biology.[61]

Historically, anticipating and comprehending biological procedures and intricate chemical reactions have presented substantial obstacles. The advancement of MD techniques has proven crucial in tackling these complexities, providing comprehensive insights into the dynamics of molecular systems. MD's significant contribution to scientific knowledge development was accredited in 2013 when the Nobel Prize in Chemistry was granted to Martin Karplus, Michael Levitt, and Arieh Warshel for creating multiscale models for intricate chemical interactions. This achievement showed how important MD simulations are for the latest information about chemical and biological processes. Molecular dynamics modelling now uses predictive technologies like machine

learning to make force fields that are accurate to the quantum level.[62]

1.3.2. The Basic Algorithm of MD

By solving Newton's classical equations of motion, MD simulations show how individual atoms move within a system over time.[63] The system's evolution, which is shown by its trajectory, demonstrates how the atoms move over a certain period of time. The simulation starts with a fixed initial arrangement, which sets the particles' exact positions in a simulation box. After that, interaction potentials are used to figure out how the forces acting on each atom from the other atoms in the system change the motion and arrangement of the all particles.[64]

The acceleration of the particles is determined using Newton's equations of motion, which is used to estimate speeds and change coordinates at later times, by integrating these equations.[64] Newton's second law of motion describes the basic theory, which is written as:

$$a_i = \frac{F_i}{m_i} = \frac{dv_i}{dt} = \frac{d^2 r_i}{dt^2} \tag{1.1}$$

The variables in Equation 1.1 are the force on the particle i represented by F , time t, acceleration a , velocity v, atomic position r, and mass of the particle m. In MD simulations, the above equation tells us how to predict the paths of atoms. After the starting conditions $r_i(t_0)$, $v_i(t_0)$, $U(r_i)$ and Δt are set, the forces for this exact timestep are found using following steps.

$$a_i = \frac{F_i}{m_i} \tag{1.2}$$

$$F_i(r_i) = -\nabla U(r_i) \tag{1.3}$$

Numerical integration of Newton's equations of motion can be used to find out where each atom is and how fast it is moving. Integration methods that are used to solve Newton's equations of motion make this purpose are the Velocity-Verlet integrator method[65] and the leap-frog stochastic dynamics integration technique[66] in MD simulation calculations, the older model being the most popular choice because it is faster to compute

and more accurate. These methods are necessary to correctly predict movement at every time step.

Through the Taylor series expansion, it is possible to guess where a particle will be in the next period of time. For the i-th particle, the position r_i at time $t + \Delta t$ is expanded as Equation (1.4):

$$r_i(t + \Delta t) = r_i(t) + v_i(t)\Delta t + \frac{1}{2}a_i(t)\Delta t^2 + O\Delta t^3 \quad (1.4)$$

The current position $r_i(t)$, the velocity $v_i(t)$, the acceleration $a_i(t)$, and time step Δt are then used in Equation (1.5) to estimate the speed and acceleration of all particles, which allows modelling of particle motion. This expansion is what integration methods for MD models are built on.

$$v_i(t + \Delta t) = v_i(t) + \frac{1}{2}a_i(t)\Delta t^2 + O\Delta t^3 + \frac{1}{2}a_i(t + \Delta t)\Delta t^2 \quad (1.5)$$

The basic structure of the Velocity-Verlet method is shown in Equation (3.5). This method moves forward by solving Equation (1.4) and getting the acceleration term from the potential energy at the new position $r_i(t + \Delta t)$ is represented as:

$$a_i(t + \Delta t) = -\frac{1}{m_i}\nabla U\big(r_i(t + \Delta t)\big) \quad (1.6)$$

In the Equation (1.6) ,$a_i(t + \Delta t)$ particle's acceleration at new time of $(t + \Delta t)$, m_i is particle's mass, and $U\big(r_i(t + \Delta t)\big)$ is the system's potential energy at the new particle coordinates $r_i(t + \Delta t)$. Newton's second law proves that the force acting on the particle will have a negative slope of the potential energy ∇U . The velocity-Verlet method is used to make sure to keep the exact integration of the equations over time. Once new acceleration is found using this equation, the updated position is calculated using Equation (1.4) which is used to predict the new speeds and coordinates over and over again for each time step. This process ensures that the equations of motion are always being integrated, which speeds up the simulation's time progress.

The system's trajectory calculated by MD simulation will depict the nanoscale change in coordinates and particle speeds over time. The mathematical models in the software will also provide the thermodynamic parameters of the system, including the energy, pressure, and various other variables. MD simulations are used to out the changes

in polymers' binding free energy or examine the forces and mechanisms underlying structural modifications in biomolecules.

To calculate the time scale sequence of molecular movements, MD simulations require certain thermodynamic parameters. These parameters will help in understanding the molecular-level relationships between the particles of the whole system; these include the overall energy of the system, its volume, temperature, and pressure. The collection of all statistical possible systems, which have the same thermodynamic properties and physical attributes at the quantum scale, is called an ensemble. In MD simulation, commonly used ensembles are detailed in the following figure:

Table 1. Common thermodynamic ensemble employed in MD

Canonical Ensemble: (NVT)	This ensemble maintains the same number of particles, volume, and temperature, rendering it appropriate for examining equilibrium characteristics under stable thermal settings.
Isothermal-Isobaric Ensemble: (NPT)	This ensemble keeps the same number of particles, pressure, and temperature, commonly utilised to replicate genuine settings characterised by changes in temperature and pressure
Microcanonical Ensemble: (NVE):	This ensemble maintains fixed particle number, volume, and total energy, making it suitable for examining systems shielded from external disturbance.

These ensembles set the foundation for outlining the behaviour of the system in molecular dynamics simulations and are essential for guaranteeing a precise picture of thermodynamic parameters.

1.4. Force Field

A force field is a mathematical model that gives the total energy of a molecular system according to its conformation. It shows large groups of atoms held together by elastic forces that can be understood through potential energy expressions. These functions consider numerous structural and interaction characteristics, encompassing bond lengths, bond angles, and non-bonded interactions. The parameters employed in force field functions are obtained from test data and advanced quantum mechanics computations.[67] These parameters warrant the precise depiction of molecular interactions, allowing the force field to consistently simulate a system's architectural, energetic, and dynamical characteristics. The system's overall energy is expressed as a sum of these potential energy components. The phrase "force field" is occasionally called "potential" in academic literature, underscoring its pivotal function in molecular modelling and simulation.[57] The above theoretical framework serves as the basis of the simulation of molecular behaviour and the prediction of system energetics.

The acceleration of a particle is calculated as the negative derivative of the potential energy function about the particle's position, divided by its mass, as specified in Equation (1.6). The overall force exerted on the atom is expressed as the change of the potential energy concerning the particle's position:

$$F_i = \sum_{j \neq i} f_{ij} \tag{1.7}$$

$$f_{ij} = -\nabla U_{ij} \tag{1.8}$$

Where f denotes the force between the respective atom and other atoms, and U signifies the potential energy function.[68] The potential energy includes both bound (bond, angle, dihedral) and non-bonded (electrostatic and van der Waals) interactions among the atoms, as specified by the subsequent equations:

$$E_{TOTAL} = U_{BOND} + U_{ANGLE} + U_{DIHEDRAl} + U_{ELECTROSTATIC} + U_{VANDERWAAL} \tag{1.9}$$

Equation (1.9) encompasses potential energy values that account for interactions among covalently bound atoms, including the two-body spring bond, three-body angular bond, and four-body torsional (dihedral) angle. These phrases outline the interactions

among atoms within a molecule. Furthermore, non-bonded atomic interactions, including the Lennard-Jones potential and electrostatic potential, are incorporated, depicting the interactions between atomic pairings (i, j), excluding those pairings already encompassed in the bonded terms.

Force fields are classified according to their origin, some of which were derived from data collected through experiments, such as X- Ray diffraction research, whereas others originate from mathematical techniques such as quantum mechanical calculations. Although most force fields employ comparable mathematical frameworks, they frequently vary in the particular equations and approaches employed to derive their parameters. Prominent examples of established force fields comprise CHARMM (Chemistry at Harvard using Molecular Mechanics)[69], AMBER (Assisted Model Building with Energy Refinement)[70], OPLS (Optimized Parameters for Large-scale Simulations)[71], GROMOS (Groningen Molecular Simulation)[72], and MMFF (Merck Molecular Force Field)[73].

1.4.1. CHARMM Force Field

Chemistry at Harvard using Molecular Mechanics (CHARMM) is a commonly used software application intended for molecular dynamics simulations. It offers a wide range of features for creating and implementing force fields critical to modeling molecular systems. CHARMM, created by Martin Karplus and his research team, has undergone continuous refinement and expansion since its establishment in 1983.[74]

The MacKerell Laboratory consistently upgrades and enhances the CHARMM force fields to guarantee their relevance and precision in molecular simulations. The CHARMM force fields offer a comprehensive database for the modeling of an array of biological substances, such as peptides, proteins, nucleic acids, lipids, and carbohydrates. These force fields are adept for both tiny molecules and macromolecules, facilitating the investigation of diverse systems. Prominent instances encompass CHARMM36 for proteins and CHARMM27 for nucleic acids, rendering them extremely effective at examining the dynamics and interactions of intricate bio-molecular systems, including polymers such as PEG and POEGMA in aqueous settings.[69] The potential energy function of the complete system is represented as:

$$U = \sum_{bond} k_b(r - r_0)^2 + \sum_{angles} k_\theta\left(\theta - \theta_{eq}\right)^2 + \sum_{dihedrals} k_\varphi(1 + cos[n\phi - d])$$
$$+ \sum_{impropers} k_\omega\left(\omega - \omega_{eq}\right)^2 + \sum_{Urey-Bradley} k_u(u - u_0)^2 +$$
$$+ \sum_{non-bonded} 4\epsilon\left[\left(\frac{R_{min_{ij}}}{r_{ij}}\right)^{12} - \left(\frac{R_{min_{ij}}}{r_{ij}}\right)^{6}\right] + \frac{Cq_iq_j}{\epsilon_0 r_{ij}} \quad (1.10)$$

1.4.2. Bonded PE Terms

Figure 1.3 shows a graphical representation of potential energy, which is related to this harmonic vibration. Oscillation about an equilibrium bond length, (r_0), arises from the force that restores equilibrium applied by the bond, defined by a bond constant (k).

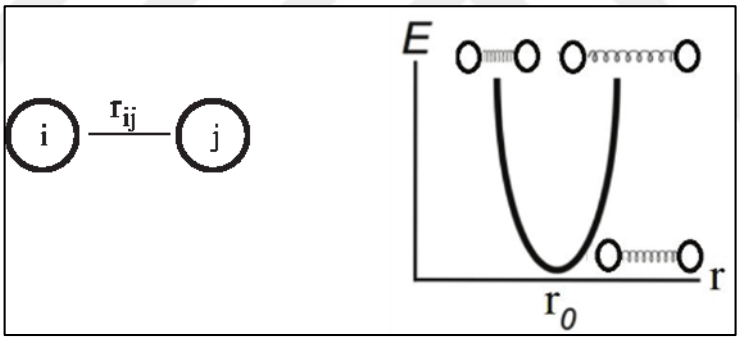

Figure 1.3 Bond Stretching and Associated Potential

The force in question emerges when the bond's length diverges from its equilibrium value, resulting in harmonic motion(vibrations) of the molecule. It is frequently represented by Hooke's law as Equation (1.11):

$$U_{bond} = k(r_{ij} - r_0)^2 \quad (1.11)$$

where U_{BOND} refers to the bond stretching potential, r_{ij} describes the instantaneous bond length, r_0 denotes the equilibrium bond length, and k denotes the bond constant, indicating the rigidity of the bond. This equation demonstrates that the

bond's behaviour is similar to a spring, with energy increasing exponentially as the bond is elongated or contracted from its position of equilibrium.

Figure 1.4 shows the angular potential, which is represented in Equation 1.12 by as U_{ANGLE} , which denotes the energy attributed to the bending action of three covalently connected atoms (i, j, k) around the center atom i. The bending happens when the angle θ is established between the two bonds i..j and j..k, shifts from the equilibrium angle θ_0. The potential energy escalates when θ deviates away from θ_0, because of the restoration force that attempts to preserve the angle near its equilibrium position. This type of behaviour is generally represented using harmonic potential as expressed in Equation (1.12):

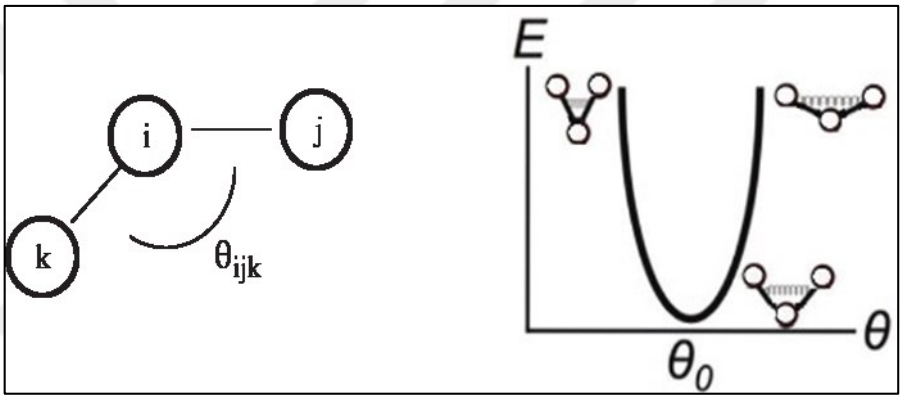

Figure 1.4 Bond energy (E) as a function of bond angle (θ) with a three-atom schematic

$$U_{angle} = k_\theta(\theta - \theta_0)^2 \quad (1.12)$$

where k_θ represents the force constant (indicating the rigidity of the bond angle) and θ_0 is the equilibrium state of the angle in radians. This equation calculates the energy expenditure associated with altering the angle between the atoms.

The dihedral potential is shown in Figure 1.5 and represented by the Equation 1.13, where $U_{dihdral}$ denotes the torsional energy caused by the rotation around the bond between atoms i and j in a set of four covalently bonded atoms (i, j, k, l). This torsional rotation changes the angle ϕ, which is defined as the angle between the planes formed by (j, i, k) and (i, j, l). The potential energy function for dihedrals is periodic and is stated as in Equation (1.13):

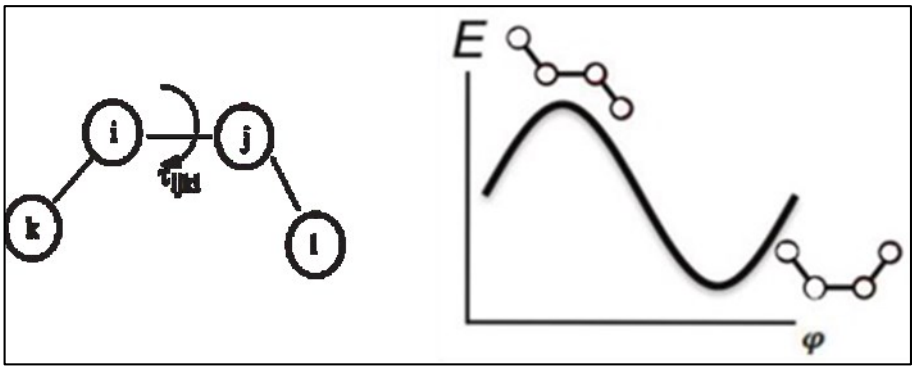

Figure 1.5 Dihedral energy (E) as a function of torsion angle (τ) with a four-atom schematic.

$$U_{dihdral} = k_\theta(1 + \cos(n\phi + d)) \quad (1.13)$$

In this context, ϕ represents the angle of dihedral in radians, n signifies the potential's periodicity (the number of minima that occur per 360° rotation), d denotes the state of equilibrium dihedral angle (the phase offset at which energy is reduced), k dictates the force constant that establishes the energy barrier's the size. The energy preference for certain torsional configurations and the obstacles to rotation around the bond are captured by this potential.

1.4.3. Non-Bonded Potentials

The Figure 1.6 below shows a graphical representation of electrostatic potential, whereas Equation 1.14 represents the formula. The $U_{electrostatic}$ denotes the interaction energy between two charged atoms i and j. It is inversely proportional to the distance r_ij between the atoms involved, implying the potential declines as the atoms move apart.

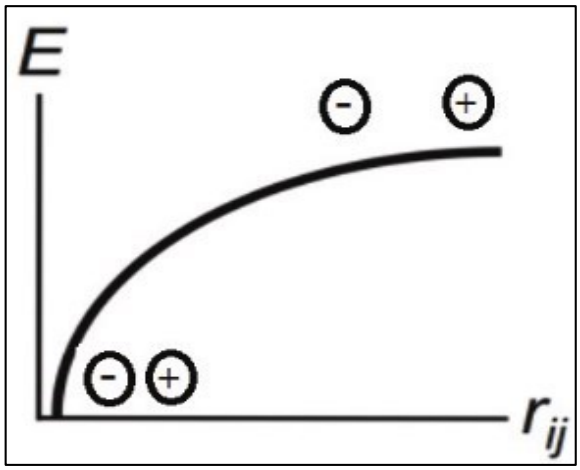

Figure 1.6 Electrostatic potential with respect to r.[85]

$$U_{electrostatic} = \epsilon_{14} \frac{Cq_i q_j}{\epsilon_0 r_{ij}} \tag{1.14}$$

The charges q_i and q_j of the atoms dictate the magnitude of the interaction, while Coulomb's constant C and the dielectric constant ϵ_0 account for the medium's characteristics. Furthermore, ϵ_14 serves as a scaling factor used to modify the interaction for 1-4 atomic pairs in molecular systems, hence ensuring a precise representation of intramolecular forces.

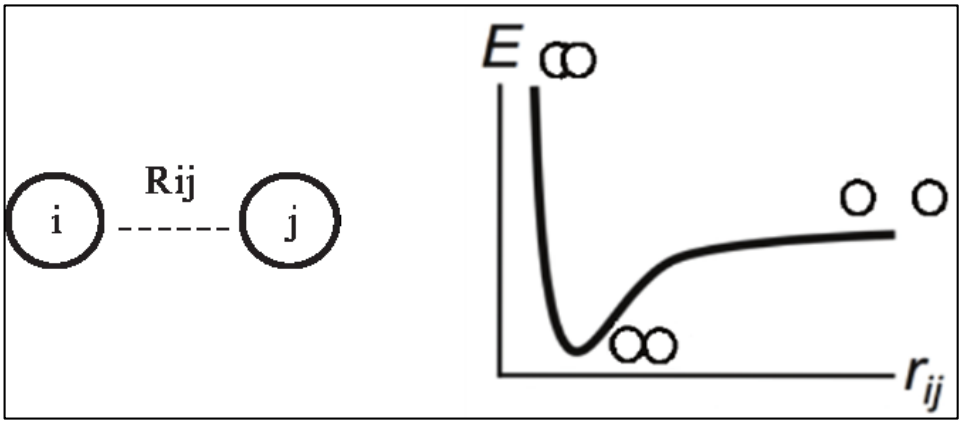

Figure 1.7 Lennard-Jones potential schematics[85]

$$U_{LJ} = -4\varepsilon \left[\left(\frac{R_{min_{ij}}}{r_{ij}} \right)^{12} - \left(\frac{R_{min_{ij}}}{r_{ij}} \right)^{6} \right] \tag{1.15}$$

The Lennard-Jones potential graph in Figure 1.7 is represented by Equation 1.15, where U_{LJ} characterizes non-bonded interactions among two atoms, equilibrating attractive and repelling forces. The attractive term signifies weak dipole-induced interactions that prevail at greater distances, whereas the repulsive term addresses the intense core repulsion when atoms are nearby. The interatomic distance r_ij dictates the intensity of these interactions. This potential elucidates the interactions of atoms inside systems, ensuring stability and realistic spatial configurations.

1.5. Problem Statement

PEG was fundamental in numerous industries, especially in pharmaceuticals, in the past, owing to its exceptional capacity to enhance the efficacy and safety of drugs. Its adaptability, biological suitability, and simplicity of chemical modifications have established it as a cornerstone in the formulation of PEGylated medicines. The pervasive application of PEG in various products, such as medications, home items, beauty products, and grooming products, has resulted in unforeseen repercussions. The primary concern is the formation of anti-PEG antibodies, which jeopardize both the safety and effectiveness of PEG-based therapies.[31] This thesis will investigate the potential of POEGMA as a viable replacement for PEG by examining the interaction of POEGMA and PEG with water through molecular dynamics modelling. Consequently, it enhances research on POEGMA by thoroughly understanding its potential.

The extensive use of PEG, previously regarded as non-immunogenic and inert, has led to frequent and long-term exposure to humans. This prolonged exposure has markedly facilitated the increase of anti-PEG antibodies, both previously present and treatment-induced. [24] Although PEG was once deemed safe, its widespread presence has elicited immunological responses that today threaten the efficacy of PEGylated pharmaceuticals. Anti-PEG antibodies pose a significant challenge for drug companies, as they can disrupt the therapeutic effectiveness of PEGylated drugs.[32] Antibody responses expedite drug elimination from the system, diminishing the pharmaceuticals' circulation and hence decreasing their efficacy.[29] Clinical research studies of PEGylated medicines, including PEG-uricase and PEG-asparaginase, have revealed detrimental consequences among patients exhibiting accelerated clearance of drugs and therapeutic failures.[75,76] The PEG-specific antibodies have been associated with acute allergic

reactions and extreme hypersensitivity during clinical research tests, which along with the other loss in effectiveness of PEG-coated drugs put the high need for researching suitable PEG alternative stealth polymers.[77]

Searching for suitable alternatives, researchers considered different polymers that are similar to PEG in non-fouling properties but without the immunogenicity of PEG. Of the various alternatives PEOGMA seems to be one of the most promising choices, because while the oligo ethylene glycol side chains still give it a biocompatible nature, the shorter length of these chains lowers the immunogenicity. The reduced immune response is attributed to short OEG branches which are hypothesized to fall below the cut-off value required for antibody detection. Moreover, unlike PEG, POEGMA can be produced by controlled polymerization methods allowing tunability and optimization of the molecular architecture hence its properties according to specific needs of the systems.[78] In addition to these POEGMA has remarkably low reactions rate and detection by PEG specific antibodies, which is necessary property in minimizing the antibody response. The reduced immune response is attributed to short OEG branches which are hypothesized to fall below the cut-off value required for antibody detection. The conformational difference between the polymers provide the possible solution to anti-PEG immune response.[78]

The improved pharmacokinetics and reduced biofouling properties prolongs the POEGMA-coated drugs lifespan in blood circulation, as a result it will reduce the dosage frequency of the drugs.[41,79] Moreover, the tunability of POEGMA allows the side chain length and the molecular size to be altered according to the requirement of the application. Preliminary studies suggest that that POEGMA conjugation increase the uptake of the drugs by the tumor, its viability and stability in biological environments, showing the potential prospect for the polymer in controlled and targeted drug delivery applications.[50,80] Furthermore, POEGMA has a much more compact molecular structure, can be taken up much better by cells and has the ability to self-assemble into nanoparticles when compared to PEG, making it an alternative next-generation stealth polymer for the pharmaceutical and biotechnology industries.[81]

Considering the potential of POEGMA as a viable alternative to PEG, it is crucial to uncover the similarities or differences between these two polymers and their underlying molecular mechanisms. This contributes to a deeper understanding of the relative advantages and limitations of POEGMA over PEG. Thus, this study aims to compare the

interaction of PEG and POEGMA with water using MD simulations. With this aim, LAMMPS software was used to perform MD simulations of different molecular weights of PEG and POEGMA in aqueous environment. Different metrics like radius of gyration, hydration shell around the polymer chain, and hydrogen bonding between polymer and water were calculated and used to compare the interactions of both polymers with water. The results of this study shed light on the differences in the interaction of POEGMA with water compared to PEG, hence provide information valuable to understand the suitability of POEGMA as an alternative to PEG for industrial and pharmaceutical uses.

CHAPTER 2

LITERATURE REVIEW

This chapter discusses pertinent scientific studies, related PEG, POEGMA, and MD simulations of these polymers, to present the previous research done in the field and gain a deeper understanding of the polymers' conformational behavior.

2.1. PEG

Tasaki et. al. utilized molecular dynamics simulations to investigate the conformation and water interactions of a polyethylene glycol chain consisting of 15 ethylene oxide units at 300 K and 373 K, corresponding to ambient temperature and the LCST of PEG, respectively.[82] The study utilized a modified force field with adjusted atomic charges and torsion terms to accurately capture PEG-water interactions and conducted the simulations in a cubic water box under NVE conditions with periodic boundaries and a long-range interaction cutoff of 8 Å, for 2 ns at 300 K and 1 ns at 373 K. Results demonstrated a transition of the PEG chain from a collapsed gas-phase conformation to a stable helical structure in water, which persisted across both temperatures. The helix featured predominantly gauche conformations around C-C bonds and trans conformations around C-O bonds, forming a (11/2) helical structure with an average pitch of 16 ± 3 Å. This conformation differed from the (7/2) helix observed in crystal structures, with the aqueous helix being more compressed and accommodating water molecules within its diameter. The helical structure was found to be highly stable, reverting to its aqueous helical form after transitioning to a random coil in benzene or undergoing simulated annealing to 1000 K. This stability was attributed to the helix's compatibility with the hexagonal water structure, minimizing disruptions to the water hydrogen-bonding network. [82]Although focused on a short PEG chain, the study provided crucial insights into PEG’s unique solubility and structural properties in water, emphasizing the importance of extended simulations for higher molecular weight polymers to generalize these findings.

The study by Smith et al. [83] employed MD simulations to investigate the conformational behavior of PEG in aqueous solutions, focusing on the effects of temperature and concentration. The simulations used an NVT ensemble with systems comprising approximately 4000 atoms, including at least eight PEO polymer molecules, with polymer concentrations varying from dilute (Wp = 0.025) to concentrated (Wp = 1.00) solutions. Simulations spanned 10 to 40 nanoseconds, utilizing quantum chemistry-based atomistic potentials validated for PEG properties. Analysis revealed that local conformations, particularly the population of gauche (g) dihedral angles around C-C bonds, increased with lower temperatures and dilute conditions. Conformations were classified as hydrophilic or hydrophobic based on their interactions with water; hydrophilic tgt and tgg sequences increased with water concentration, while hydrophobic tg+g- conformations became more prominent at higher polymer concentrations. In concentrated solutions, PEO chains exhibited compact dimensions due to reduced C-C g dihedrals increase in the C-O g dihedral. In contrast, in dilute conditions, chains extended due to excluded volume effects rather than changes in local conformations. Chain dimensions exhibited weak temperature dependence, attributed to decreased solvent quality with increasing temperature[83]. These findings provide a comprehensive understanding of PEO's conformational properties in water, which are crucial for its applications in diverse aqueous environments.

Another study by Smith et al. employed MD simulation [84] to study the PEG-water interactions, focusing on hydrogen bonding and its dependence on solution composition and temperature. Systems consisted of PEG with a molecular weight of 530 Da in aqueous solutions spanning polymer Wp from 0.025 to 0.90 and temperatures from 298 K to 450 K. Each simulation included approximately 4000 atoms, using quantum chemistry-based atomistic potentials for PEG and the TIP4P model for water, with electrostatic interactions computed via Ewald summation. Simulations were conducted under NPT conditions for 2-3 ns to determine equilibrium densities, followed by NVT production runs lasting 10–50 ns. The results showed that PEG-water hydrogen bonding increased in dilute solutions but saturated at Wp = 0.5, with saturation corresponding to the stabilization of PEG-water interactions. Temperature elevation reduced hydrogen bonding, aligning with experimentally observed LCST behaviour. At immiscibility conditions (450 K), nearly 50% of PEG-water hydrogen bonds were broken. Water clustering was pronounced in concentrated solutions, and while some water molecules

formed bridges between ether oxygen atoms, these predominantly connected oxygens within the same PEG chain [84]. Thermodynamic analyses linked hydrogen bond dynamics to enthalpy and entropy changes, providing insights into the energetics of PEG-water interactions, which is critical for understanding polymer solubility and behavior in aqueous environments.

In the study by Lee et al., a coarse-grained (CG) model for PEG within the MARTINI force field was used, mapping 3–4 heavy atoms to single CG beads and refining bonded and non-bonded parameters for accurate structural and dynamic properties.[85] Chain dimensions, including the radius of gyration (R_g) and end-to-end distances, showed strong agreement with experimental and all-atom simulation results, particularly for PEG76, where CG and all-atom R_g values (19.1 ± 0.7 Å and 20.4 ± 0.8 Å, respectively) closely matched the experimental value (19.7). The model captured the transition from ideal to actual chain behaviour at Mw ≈ 1600–2000, consistent with experimental data. Simulations of PEG76 at varying concentrations revealed no significant change in R_g, suggesting that previously observed concentration dependence might be due to interchain scattering. Moreover, the simulations successfully modelled the mushroom-to-brush transition as grafting density increased in grafted PEG aligning with Alexander-de Gennes' theory[85]. This model enables efficient and accurate simulations of PEG in various environments.

Lee et al. employed MD simulations to investigate the behaviour of PEO and PEG in aqueous solutions, focusing on validating the revised CHARMM ether force field and analysing polymer conformations and hydration effects[86] (Lee et al. 2008). The C35r force field demonstrated excellent agreement with experimental conformer populations. Simulations were conducted using the TIP3P water model at 296 K and 1 atm, employing a Nosé-Hoover thermostat, Andersen-Hoover barostat, and particle mesh Ewald (PME) for electrostatics. Polymers of different lengths (-9, -18, -27, and 36-mers and 27-mers of PEG were simulated in water boxes with dimensions ranging from 44 Å to 58 Å per side. Chain dimensions, including the radius of gyration (R_g) and end-to-end distances, confirmed that PEG behaved as an ideal chain at low molecular weights, with a persistence length of 3.76 ± 0.4 Å, matching experimental values. Hydrodynamic analyses revealed that hydration significantly influenced the hydrodynamic radius (Rh), $Rh \approx 0.85\ R_g$ was observed for PEG molecules, the theoretical value of which is 0.665 derived from the Kirkwood-Riseman model for an ideal chain. This difference can be

attributed to the presence of the hydration shell. The study further noted shape anisotropy, where the middle dimension of PEG chains was slightly smaller than 2Rh of membrane pores, correlating with polymer diffusion through membrane pores[86]. These findings affirm the suitability of the C35r force field for simulating PEG in water and provide valuable insights into polymer hydration and transport behaviour.

The study by Oelmeier et al.[87] carried out MD simulations using the Yasara Structure software package with Amber03 force field to investigate the effect of PEG chain length on its structure and interactions with water, providing insights into its behavior in aqueous two-phase systems (ATPS). Simulations were performed for 10-30 ns in a TIP3P water system at 298 K and pH 7.0, utilising rectangular simulation boxes customized for PEG lengths. Structural research indicated that PEG assumed a random-coil shape, exhibiting increased helicity and hydrophobic surface exposure with longer chain lengths due to greater accessibility of CH groups. The polymer's R_g increased as its molecular weight was increased, meaning the polymers behaved like ideal polymer chains. At the same time, the surface became more hydrophobic, meaning there were fewer hydrogen bonds between PEG monomers and the water structures around them. The surface hydrophobicity that was observed in the simulations matched well with lab phase-separation data and experimental solvent polarity tests. This proved that the simulation framework was a reliable way to show how PEG and water interact at the molecular level [87]. These results show how chain length affects the surface properties of PEG, how it shapes the water layer around the chain and its interaction with solvents, which are important for its use in ATPSs and precipitation of proteins.

Kaiser et al. conducted molecular dynamics simulations utilizing the OPLS-AA force field to investigate the hydrogen-bond network of ethylene glycol (EG)[88]. A cubic periodic box with an average density of 1.1003 g/cm³ was used for simulations. Equilibrated simulations were performed under NVT and production runs using NPT ensembles for 1 ns. To gain insight into hydrogen bonding behavior, they developed molecular visualization tools to study the start, formation and breakdown of hydrogen bond structures in liquids, providing new insights into their transient behaviors and structural arrangement. The hydrogen-bond study indicated that EG established an average of 3.7 ± 0.2 bonds between molecules per molecule, characterized by spontaneous splitting and reformation, resulting in a brief bond lifespan of 1.5 ps and diffusion-related longer-term dynamics of 80.3 ps[88]. Visualization methods showed

hydrogen-bond networks' transient nature. The study shows how important it is to select the appropriate forcefield parameters to correctly demonstrate the PEG's conformational and molecular properties, it also provides insights into hydrogen-bonding behaviour in PEG-water interactions.

The article by Hoffmann et al.[89] explored the impact of water impurities on the properties of PEG200 and its oligomers (di-, tetra-, and hexaethylene glycol) through MD simulations were performed using a combination of SPC/E and TIP4P/2005 water models with GROMACS, using OPLS-AA force field. The systems were kept at 328 K, and 1 bar, 500–1000 oligomer molecules with mass fractions 0 to 0.02 were used. Following energy minimization, the systems were equilibrated in the NPT ensemble, and then the NVT ensemble was used for production runs. The results showed that the polymer did not aggregate but rather formed hydrogen bonds with the water structure around it; the hydroxyl and ether groups interacted with water molecules, preserving constant water-PEG interaction profiles across water concentrations. The radius of gyration and end-to-end distances of the polymers changed slightly as the water concentration was increased. Simultaneously, RDFs, including water, revealed consistent interaction between water and PEG, with water concentration having no effect on these interactions.[89] Comparison with experimental data indicated possible overestimations of hydrogen bonding strength in simulations, as physical properties showed slight deviation from experimental results, including minor changes in density, self-diffusion coefficients, viscosities, and heat capacities. These results provided a qualitative understanding of how water affects PEG and oligomer properties.

2.2. POEGMA

The research conducted by Ozer et al. [81] investigated POEGMA as a stealth polymer substitute for PEG, emphasizing its chemical structure and its impact on biological interactions. Employing RAFT polymerization, the authors produced POEGMA10K and POEGMA20K, contrasting them with commercially acquired PEG10K and PEG20K. Dynamic light scattering (DLS) measurements revealed the compact structure of POEGMA, evidenced by its reduced hydrodynamic diameter (Dh) in water relative to PEG. In contrast to PEG, POEGMA had notable interactions with serum proteins, as indicated by elevated Dh in PBS and serum-containing medium,

corroborated by surface plasmon resonance (SPR) spectroscopy revealing considerable serum adsorption on POEGMA. Atomic force microscopy (AFM) demonstrated that POEGMA10K self-organized into nanoparticles owing to its distinctive hydrophobic and hydrophilic interactions, a characteristic lacking in PEG. Cellular investigations revealed that POEGMA exhibited enhanced absorption by BEAS-2B and A549 cell lines, driven by energy-intensive mechanisms and caveolae-mediated endocytosis, a phenomenon not found with PEG. Furthermore, in contrast to PEG, POEGMA demonstrated less steric hindrance, hence facilitating the absorption of biomolecules, including integrin-targeting peptides.[81] These research results emphasized the difference of POEGMA when compared with PEG, such as enhanced penetration into cells, self-assembly properties, and superior targeting potential, underscoring its significance for drug delivery applications.

The research conducted by Qi et al. [78] emphasises the capability of POEGMA attachment to improve the pharmaceutical efficacy of therapeutic peptides, utilising exendin-4 as a model medication for type 2 diabetes mellitus. Unlike the original exendin, which only worked for six hours, the exendin-C-POEGMA conjugates lowered glucose levels in diabetic mice for up to 120 hours after a single injection under the skin, which is significantly longer duration. Increasing the molecular weight of the POEGMA chains not only extended the drug activity time, but it also made it less likely for the conjugated drug, to bind to receptors. This shows the importance of finding the best chain length to balance drug effectiveness and how long it circulates in the blood. EG3 exendin-C-POEGMA combinations had shorter side chains, but they were just as effective as EG9 variants. They also had less immunogenicity, showing the tunability of POEGMA properties to lower the risk of an antibody response without losing their therapeutic benefits. The researchers used sortase-catalyzed technique to make very accurate and large amounts of site-specific, flexible molecular-weight POEGMA conjugates. [78]. The decreased antigenic properties of POEGMA, along with its capacity to extend circulation durations and enhance drug delivery, position it as an appropriate substitute for PEG for improving the stability and effectiveness of therapeutic peptides and proteins.

Sano et al. assessed the effectiveness of POEGMA as a tumour-targeted drug delivery system via both in vitro and in vivo tests [50]. Using atom transfer radical polymerization (ATRP), the POEGMA derivatives with molecular weights of 11, 21, and 30 kDa and different EG side chain lengths were synthesised. For biological dispersion

tags, indium-111 was used, and indocyanine green (ICG) tags were used for image analysis of the compounds. Cell penetration of the conjugates was studied using fluorescence microscopy, which showed that colon26 tumor cells were penetrated by ICG-labeled POEGMA compounds more easily than PEG-labeled compounds. Compared to higher molecular weight derivatives, POEGMA-B (21 kDa) had better tumour uptake and better tumour-to-normal tissue ratios in colon26 tumour-bearing mice. This was because it had longer circulation within the body and less off-target buildup in the liver and spleen. Compounds with shorter EG side chains were less likely to aggregate in stomach [50]. The results show that POEGMA-B (21 kDa) is a good choice for delivering drugs to tumors because it balances better targeting of tumors with fewer side effects that aren't supposed to happen. It can also be used in cancer diagnosis and treatment.

The research of Gao et al. [90] proposes conjugating protein-based medicines with POEGMA to improve their therapeutic characteristics. POEGMA is comparable to PEG but has significant drug delivery advantages. This approach used in this research demonstrates that adding POEGMA improves green fluorescent protein's efficacy and therapeutic properties (GFP). In blood exposure (AUC), the GFP-POEGMA conjugate's hydrodynamic radius (Rh: 21 nm) rose 15 times in comparison with unchanged GFP (Rh: 3.1 nm) and its terminal elimination lifetime was much longer, indicating lower body removal and longer circulation time. POEGMA conjugation also increased tumour targeting through the enhanced permeability and retention (EPR) effect in cancer-bearing mice, resulting in a 50-fold increase in tumour accumulation for the GFP-POEGMA combination in comparison to protein[90]. This shows that the polymer improves circulation time and site-specific distribution, which are crucial for cancer treatment. This study shows that POEGMA could replace PEG for future protein-based medicinal treatments.

Cheng et al. utilized Small Angle Neutron Scattering (SANS) to investigate the structure and clustering actions of a polymer featuring a polystyrene backbone and abundantly attached OEG side chains providing insights into a polymer similar to POEGMA [91]. The research generated PTrEGS polymers with backbone polymerization degrees of 8, 40, 47, 58, and 85 while retaining an OEG side chain length of 4 and used Toluene-d8, methanol-d4, and D2O to study polymer behaviour. Zimm analysis of the second virial coefficient (A2) for the longest chain (DP = 85) showed good (toluene-d8), marginal (methanol-d4), and bad (D2O) solvent environments. As DP was raised, the polymers evolved from rigid to semiflexible cylindrical configurations in good and

marginal solvents, improving mobility in longer chains and preserving rigidity in bad solvents because of hydrophobic backbone collapsing. Shorter chains clustered in all solvents due to hydrophobic end-group interactions and OEG side chain D2O hydrogen bonding [91]. Research on solvent-dependent structure and aggregation reveal that polymers like POEGMA may adapt to changing environmental situations, giving them greater control and utility than PEG. Because it has a hydrophobic backbone and the identical OEG side chains as POEGMA, results have shed light on its structural conformation in different solvents.

The experimental approaches utilized to analyze POEGMA's characteristics and structural behaviour Liu et al. demonstrate its adaptability in numerous applications.[41] Turbidimetry, NMR, DLS, and AFM are used to study POEGMA's thermosensitivity, molecular assembly, and non-fouling characteristics with a high resolution. Key results from research show that POEGMA's LCST is affected by side-chain length, with larger side chains reaching higher cloud points because of enhanced hydration capacity. The work also shows that co-polymerizing monomers with different side-chain lengths may optimize the LCST for accurate temperature-responsive behavior. POEGMA's structure-dependent molecular assembly, driven by side-chain collapse, generates mesoglobules and micelles. These structures, affected by concentrations of polymers and temperature, could be used in medication delivery. POEGMA brushes discourage protein adhesion, making them non-fouling. Chain structure affects protein-repellent ability and porousness[41]. POEGMA's UCST in alcohols, controlled by backbone length and end-group changes, shows its adaptability to different conditions.

Johnson et al. synthesized a P(MEO2MA-stat-OEGMA300) copolymer brush with 80 mol% MEO2MA and 20 mol% OEGMA300 to study POEGMA brushes' thermoresponsiveness. Using neutron reflectometry (NR) and quartz crystal microbalance with dissipation (QCM-D), they evaluated the brush's reactions to fluctuations in temperature and potassium acetate (KCH3COO) and potassium thiocyanate (KSCN) electrolyte solutions [92]. NR exhibited brush hydration, density, and thickness at the nanoscale, while QCM-D disclosed viscoelasticity and swelling/collapse changes. The brush's temperature of transition climbed with OEGMA300, showing its thermoresponsiveness. Chaotropic thiocyanate ions enhanced swelling and transition temperature, while acetate ions decreased it. Acetate's impact decreased at greater temperatures due to steric barriers in the crashed polymer, while thiocyanate kept

interacting with it. These findings demonstrate POEGMA's versatility, making it a promising material for applications requiring flexible and adjustable temperature and ionic properties.

MD simulations can be used explain POEGMA's LCST responses in aqueous settings. Dalgakiran and Tatlipinar used molecular dynamics simulations to study POEGMA300's water solubility and lower critical solution temperature, concentrating on hydrophobic hydration [48]. The General AMBER Force Field (GAFF) determined partial atomic charges, and the TIP3P water model in an octahedral periodic box simulated the solvent setting. The trajectory and energy measurements were gathered every 5000 steps to study the polymer's temperature-dependent characteristics at 290 K, 307 K, 330 K, and 350 K during 100-140 ns production cycles The simulations showed that POEGMA300, with a polymerization of 20 or higher, undergoes a coil-to-globule transition above its LCST due to hydrophobic hydration activities around the side chain carbon atoms. Water molecules formed cage-like structures surrounding hydrophobic side-chain carbons below the LCST, increasing polymer solubility. These aqueous arrangements decomposed at temperatures over the LCST, disclosing the polymer's hydrophobic regions and causing clustering. The size loss during this transition is greater with longer backbones but less with longer side chains. Compared to hydrophobic hydration, hydrogen bonding between the polymer and water had little effect on the LCST phase transition. Due to hydrophobic hydration structure collapse and polymer conformational shift, longer polymer chains (e.g., 50-mer and 75-mer) have a lower coefficient of diffusion with increasing temperatures. [48].

Dalgapınar et al. performed MD simulations to examine the LCST behavior of a diblock copolymer consisting of PMEO2MA and POEGMA300 in aqueous environment, utilizing the Amber14 software with GAFF force fields and partial atomic charges obtained via ab initio computations [93]. In TIP3P water, periodic boundary conditions were used to mimic single-chain copolymer systems with block ratios of 20/5, 20/20, and 50/20 in a truncated octahedral box. Minimization, heating to 290 K, equilibration at 1 atm, and production runs at 290 K, 307 K, and 330 K for 200 ns were performed. $R_{g,}$ hydrogen bonding, water arrangement around the polymer, and hydration behavior were examined. The breakdown of hydrophobic water structures enclosing the sC enhances entropy and facilitates the LCST transition, causing coil-to-globule conversions at 307 K for PMEO2MA and 330 K for POEGMA300[93]. These research results emphasize

hydrophobic hydration and water cage collapse in LCST transitions and inform thermoresponsive polymer design.

Heather et al. used MD simulations to study a polymer's self-assembling process and properties with POEGMA, MAA, and anthracene units[94]. The research analyzed polymer-solvent interactions, including hydrogen bonding, π-π interactions, and hydrophobic effects in different solvent settings. The GROMOS 54a7 force field with Automated Topology Builder 3.0 parameters were used for modeling single-chain syndiotactic 25-mers with MAA, 5 evenly spaced POEGMA 8-mers, and variable anthracene units (0, 2, 4, or 8). Computations were conducted in GROMACS 2018.3, using 20 chains in a 10 nm^3 box with pre-equilibrated solvents (water, THF, or DMF). A 500-ns NPT ensemble analysis of solvent-accessible surface area (SASA), hydrogen bonding, and anthracene-anthracene interactions revealed compositional and solvent influences on polymer assembly. In water, POEGMA's hydrophilic character maintained solubility and MAA accessibility, but increasing anthracene content lowered SASA and intra-polymer hydrogen bonding, favouring hydrophobic aggregates.[94]. Notably, POEGMA counterbalanced this hydrophobicity by preserving hydrophilic domains. In THF, the absence of anthracene favoured hydrogen bonding among MAA units, which decreased as anthracene increased, leading to dominant hydrophobic interactions. In DMF, polymer-solvent interactions were predominant, but some intra- and inter-chain interactions persisted. These findings demonstrated POEGMA's critical role in modulating solvent-dependent self-assembly, providing structural stability, and balancing hydrophilic and hydrophobic interactions, underscoring its potential for applications such as drug delivery.

CHAPTER 3

COMPUTATIONAL AND ANALYSIS METHODOLOGY

In this chapter the simulation methodology i.e. the molecular modelling, the system setup and simulation parameters as well as the analysis methodologies i.e. radius of gyration, watershell analysis and hydrogen bond analysis will be discussed.

3.1. Molecular Design and Configuration

3.1.1. PEG

The initial structure for different lengths of PEG solvated in various sizes rectangular simulation box with TIP3 water molecules was done using Polymer builder in CHARMM-GUI.[95] CHARMM-GUI Polymer Builder simulates and generates well-equilibrated polymer configurations. The "solution" system option can solvate polymer chains into the available solvents and set up an MD simulations system. In the first step, PEG polymers were constructed using monomer units that were solvated in different-sized TIP3P water boxes.

In the next step, it divides the polymer into CG beads according to the length of the monomer units and performs a CG simulation to equilibrate the system, and then the beads are replaced with atoms. Lastly, the complete topology with CHARMM force field parameters and simulation input files for LAMMPS were generated. PEG of 20 and 40mers were constructed with CHARMM forcefield parameters in simulation box size of (100*100*100) cubic Angstrom for 20 and 40mers.

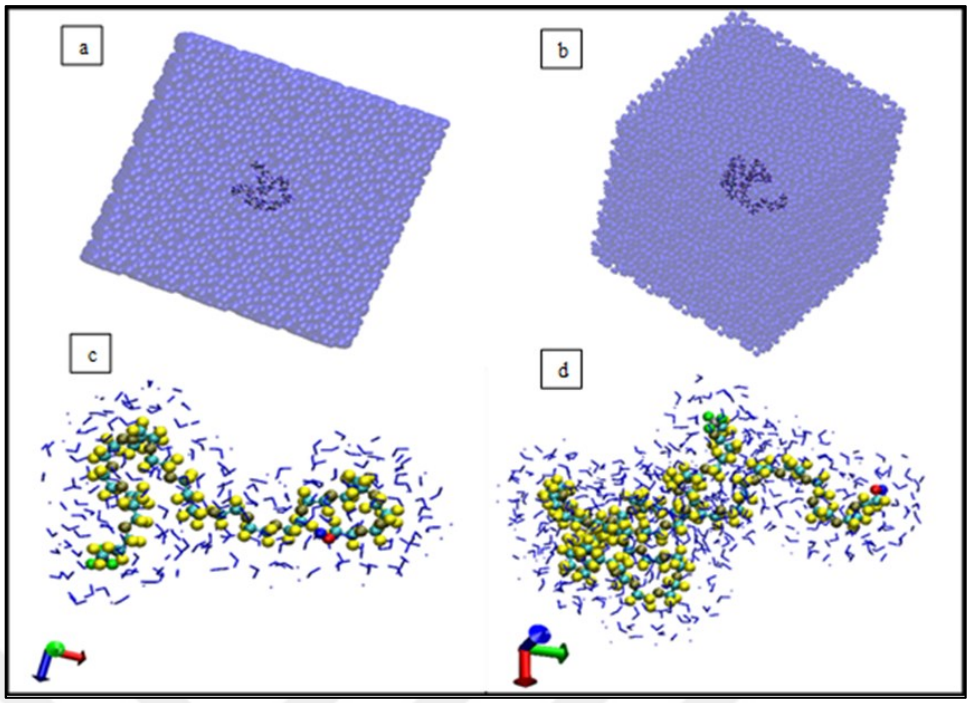

Figure 3.1 (a) PEG20 and (b) PEG40 in water box, (c) PEG20 and (d) PEG40 molecular model surrounded by water molecules.

3.1.2. POEGMA

The molecular structures POEGMA having 4-, 8-, 12-, 16- and 20 repeating units (degree of polymerization) with side chains of 5 OEG repeating units, were designed using Avogadro molecular editing software[96], the pdb and mol2 file from Avogadro was used to generate LAMMPS data file using Open Babel software[97], CGenFF was used to get the CHARMM forcefield parameters for the data files.[98] The (100*100*100 Angstrom) cubic TIP3 water box was generated separately for each polymer in LAMMPS.[99,100] The polymers were solvated, and polymer water mixture data files with charmff parameters were generated and used in the simulations., Figure 3.2 shows their initial structures solvated in water.

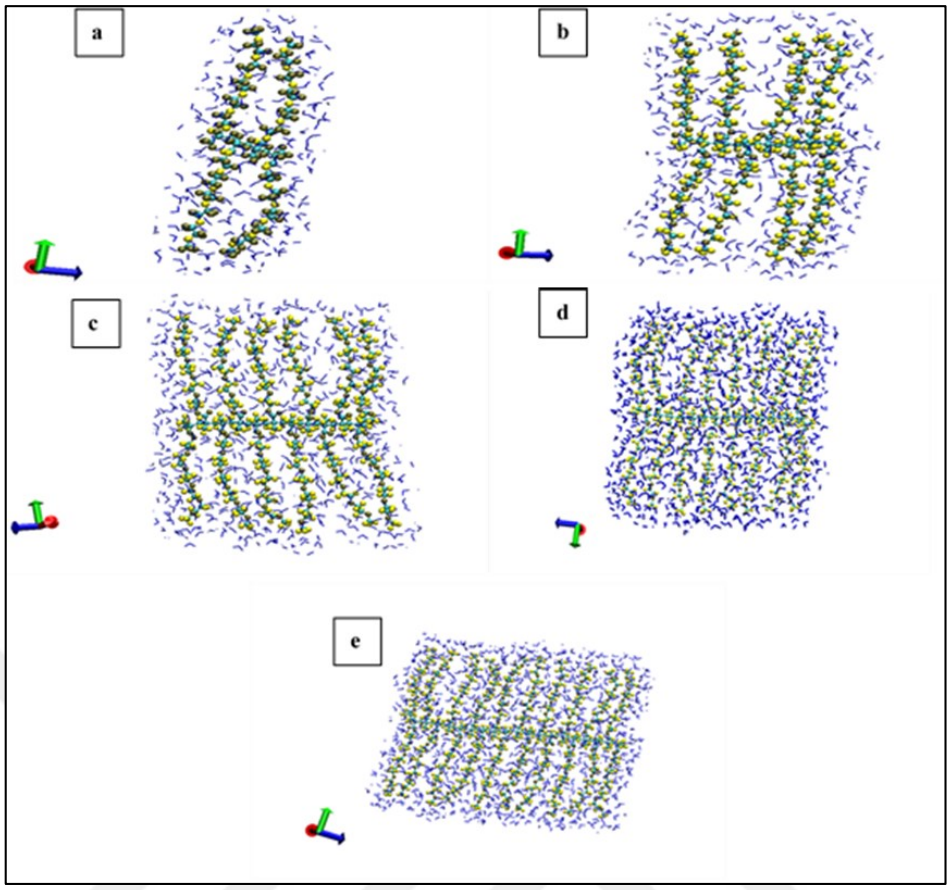

Figure 3.2 (a) POEGMA4, (b) POEGMA8, (c) POEGMA12, (d) POEGMA16 and (e) POEGMA20 initial molecular model surrounded by water molecules

3.1.3. Simulation Parameters

The MD simulations were performed on LAMMPS using the CHARMM forcefield.[101] The simulations used a real unit system, where the unit of time was femtosecond (fs), the unit of distance was in Angstroms (Å), and the unit of energy in kcal/mol. Periodic boundary conditions were used to simulate the system and avoid edge effects, where atoms exit from one side of the box to re-enter the side. Before the simulation started, Newton's third law was disabled using “newton off” to enhance stability during and ensure accurate force evaluations even in complex molecular systems. A combination of Lennard-Jones and Coulombic potentials was used through “lj/charmmfsw/coul/long pair style” to simulate the non-bonded interactions where the min cutoff distance was 10 Å and max distance of 12 Å to make sure energy and force

transition at the boundary was smooth ensure smooth force and energy transitions at the cutoff distance. The interactions between all the particles were achieved using "pair_modify mix arithmetic" command. Long-range Coulombic interactions were calculated using the particle-particle particle-mesh (PPPM) method, achieving an accuracy of 1×10^−6 kcal/mol by the command "kspace_style pppm 1e-6".

The full atom style was used for molecular representation of all the atoms in the system, to ensure that all the attributes like angle, dihedral, and improper and charge descriptors were included. The harmonic potentials using "bond_style harmonic" modelled the bonded interactions, angular interactions were modelled using "angle_style charmm" command, while CHARMM force-switching potential was used to model dihedral rotations using "dihedral_style charmmfsw" command, and harmonic potentials were employed to describe improper torsions using "improper_style harmonic". the timestep of 2 fs meaning that each iteration of the simulation was of 2 femtoseconds during the whole simulation.

At the start, the minimization was performed to stabilize the initial structure of the system. Before the minimization process was started, the particles in the system were assigned velocity using "velocity all create 310 83628 dist gaussian" command, which states that all atoms' velocities will be similar to the natural movement of particles at 310K temperature. Temperature control during the minimization was administered using Nosé-Hoover thermostat,[102,103] using the command "fix 1 all nvt temp 310 310 100.0", which means an NVT(canonical) ensemble, where a constant temperature of 310 K was maintained while maintaining the fixed volume with a damping parameter of 100 timesteps. After velocity and temperature control, a conjugate gradient minimization method was applied using the command "min_style cg", the minimization was executed using the command "minimize 0.0 1.0e-8 100000 200000", where the target energy tolerance was 0.0 kcal/mol and the force tolerance was 1×10−8 kcal/mol/Å. The minimization proceeded for a maximum of 100,000 iterations, with a maximum of 200,000 force/energy evaluations. After the minimization, 1 ns of equilibration was also performed with the NVT ensemble, then 15 ns of production run was performed with NPT ensemble.

3.2. LAMMPS

LAMMPS (Large-scale Atomic/Molecular Massively Parallel Simulator) is an MD simulation software developed by the US Department of Energy and other private sectors; it is currently managed and distributed by Sandia National Laboratory.[104] It is an open-source software that uses classical dynamics codes to simulate all states of material, including solid, liquid and gas. It is capable of modelling CG, macroscopic, atomic, polymeric, solid-state, biological systems and various other systems using several forcefields and boundary conditions. It can simulate both 2d and 3d systems with a vast particle number range.[101] It can be installed and run on personal computers, but it is designed for parallel computers with multiple GPU and CPU servers and distributed memory clusters. We performed our simulations on LAMMPS installed TRUBA(Türk Ulusal Bilim e-Altyapısı) HPC(High-Performance Computer).[105]

3.3. Simulation Analysis

The trajectories files (dcd and lammps data), obtained from MD simulation using LAMMPS [101] were analyzed using Visual Molecular Dynamics(VMD)[106] and python Mdanalysis[107] tool on Google Colaboratory.[108] The Radius of gyration and watershell analysis for each frame were done using VMD and hydrogen bonding analysis was performed using pro version of Google Colab.

3.3.1. Radius of Gyration (R_g)

The radius of gyration (R_g) is the spatial arrangement of the polymer atoms around it center of mass. To understand of the compactness and molecular size of the PEG and POEGMA structures comprehensively, we analyzed the R_g data for all the PEG and POEGMA -mers . It provides details about the conformation of the polymer during the simulation. R_g is calculated as the root mean square distance of the atoms of the PEG and POEGMA chains from its center of mass. R_g in VMD is calculated using ‘measure rgyr’ command. This is defined as the following equation:

$$R_g = \left[\frac{\sum_{i=1}^{N} m_i(r_i - R)^2}{\sum_{i=1}^{N} m_i}\right]^{\frac{1}{2}} \quad (3.16)$$

Where m and r are the position of the ith atom and R is center of mass position of the total number of polymer chain. To calculate the R_g, first the LAMMPS data file and dcd trajectory was loaded in the VMD, then a TCL script was ran using TK-console to get the radius of gyration for each frame of the simulation. In this script first the polymer atoms were selected based on the type of the atoms, then the R_g was calculated using the squared root-mean distance of each atom and the polymer's center of mass. This returned text file containing the radius of gyration for each frame of the simulation in Ångströms, which was used to study the conformation change of the polymer in aqueous environment. The results were analyzed using Kaleidagraph software,[109] the Tcl script is provided in Appendix A.

3.3.2. Watershell Analysis

In order to analyze the hydration behaviour of the polymer, a Tcl script in VMD was used to calculate the number of water molecules within 5.0 Å distance of the polymer molecule for every frame throughout the simulation. The script first defined the polymer and water molecules based on their atom types, then the unique number of water molecules within the cutoff distance for each frame were added to a text file. This data was to analyze the change of watershell and how it can be related to the conformation of the polymer using Kaleidagraph data analysis software,[109] the full Tcl script is provided in Appendix B.

3.3.3. Hydrogen-Bond Analysis

Hydrogen bonding is electrostatic interaction between hydrogen donor (which in our case is water hydrogen) and hydrogen acceptor (which in our case is the oxygen atom of the polymer). It plays a critical role in stabilizing the polymer structure, it is usually defined by the distance between the donor and acceptor atoms which is generally 3.5 Å

and the angle donor-hydrogen and acceptor which was greater than 135 degrees as shown in Figure 4.7.[110]

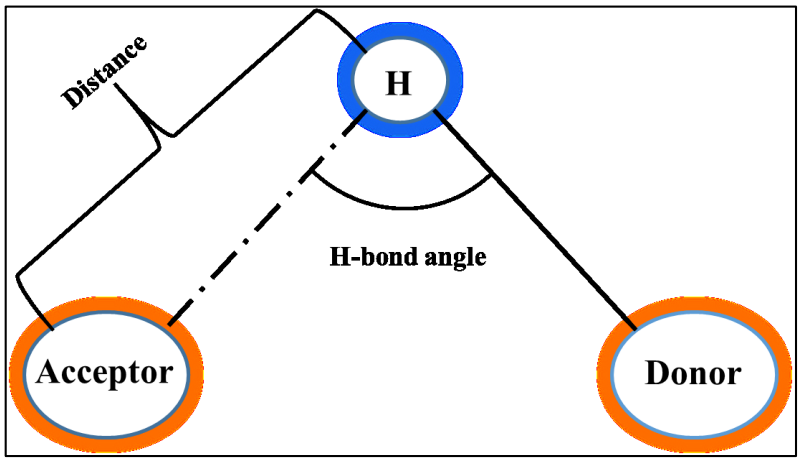

Figure 3.3 H-bond schematic showing the cutoff distance and angle

H-bonds between water and the polymer are vital in understanding the hydration dynamics and it also plays major role in the solubility of the polymer. The H-bond analysis was performed using MDAnalysis library[107] in Python on Google Colab platform. The trajectory files were uploaded to Google Drive, and the Colab was accessed to the folders containing simulation data. A Python script was used to perform the analysis, In the script, the water donor hydrogen atoms and polymer acceptor Oxygen atoms were selected based on their atom type, the cutoff distance of 3.5 Å and cutoff angle of 135 degrees were designated; the analysis were then performed for each frame of the trajectory. This gave a csv file containing the frame numbers, donor Hydrogens' indices, acceptor Oxygens' indices, donor-acceptor distances and angles for all H-bonds. Kaleidagraph software was used to analyze the data,[109] the full Python script is provided in Appendix C.

CHAPTER 4

RESULTS AND DISCUSSION

In this chapter the findings of MD simulations are presented, and the data collected for R_g, watershell and H-bond analysis of both PEG and POEGMA are provided. The findings are discussed in the context of how all are related to each other and the polymer conformation.

4.1. Radius of Gyration (R_g)

The radius of gyration graph in Figure 4.1 shows the time evolution of the R_g from the center of mass of PEG20 in blue and PEG40 in red color. The R_g of PEG20 has the lowest value of 6.72 Å at the start of the simulation and the highest value of 15.55 Å around the 800th frame, which is around 12 ns. The mean PEG20 Rg throughout the simulation is 9.73 Å, while the standard deviation from the mean is 1.61 Å , which means that for most of the simulation, the Rg is stable. The structure of PEG20 at the start is compact after the initial relaxation and it remains around the lowest value for around the first 100 frames which is until 1.5 ns, and then the structure starts to expand and Rg increases to around 14 Å around 2.25 ns, then the structure stabilizes the most part of the simulation with the occasional peaks and valleys in the value, and only goes three times near the lowest value at around 500th and 750th frame. The changes throughout the simulation can be attributed to the change in the helical random coil structure.

The R_g of PEG40 unlike PEG20 increases steadily from 9.7 Å in the first frame to its largest value of 22.47 Å at around 325th frame which is around 4.88 ns into the simulation, then it drops to the mean value which is 13.41 Å at around 450th frame which is around 6.75 ns, around that value it comparatively it oscillates, with on major drop at around 700th frame which is around 10.5 ns into the simulation. The standard deviation of R_g throughout the simulation from the mean value is 2.81 Å, which is about 60% more than the PEG20. Even though for some part of the simulation, the R_g variations are

comparable, but overall the R_g values of PEG40 are far more volatile when compared to PEG20.

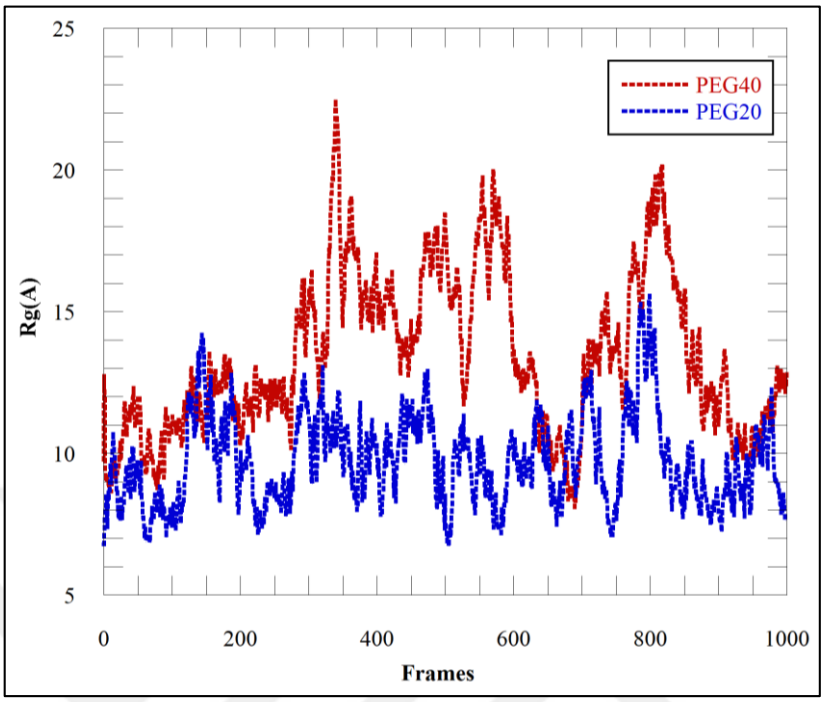

Figure 4.1 PEG20 and PEG40 Radius of Gyration.

The box plot of R_g of both PEG molecules in Figure 4.2 shows that the distribution of PEG20 R_g is more compact, shown by the smaller box size, while the PEG40 dispersed R_g distribution is shown by the bigger box size. PEG40 has a right-skewed distribution as the median value is closer to the first quartile, while PEG20 has a normal distribution as the median is in the middle of the box. Moreover, there are few outliers in both distributions.

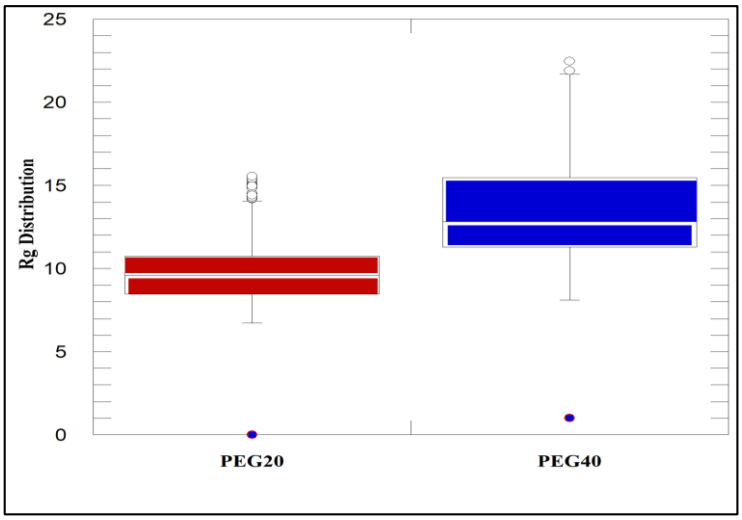

Figure 4.2 R_g distribution box plot of PEG20 and PEG40

The radius of gyration plot given in Figure 4.3 shows the time evolution of distance from the center of mass of POEGMA4, POEGMA8, POEGMA12, POEGMA16 and POEGMA20 to the outermost polymer atoms in the system. These values provide an insight into the conformation of all polymers as the simulation progresses, which can be useful in indicating the conformation behaviour like its compactness and extendedness or folding of the polymer.

The R_g values POEGMA4 does not show that much fluctuation compared to PEG20 (which has same number of EG repeating units). The initial value at frame zero was 13.10 Å, the highest R_g value was 14.03 Å while the lowest was 12.88 Å, and the mean R_g value throughout the simulation was 13.46 Å with a standard deviation of 0.181 Å. The R_g values of POEGMA8 also follows the similar trend and it does not fluctuate much from the initial. The mean R_g value is around 15.78 Å and as the minimum value of the entire 15 ns run is 14.11 Å and the maximum R_g value is 16.12 Å with a standard variation of around 0.143 Å from the mean value of the whole distribution. POEGMA12 has the mean R_g value of 17.81 Å with the minimum and maximum values of 16.12 Å and 18.19 Å, respectively. The standard of deviation for the entire distribution is around 0.146 Å from the mean value. For POEGMA16, the R_g value is stable like the others, it has the mean value of 20.03 Å with the standard deviation of 0.135 Å, which means the within 0.27 Å, lies around 68% of R_g values. Lastly, the mean R_g of POEGMA20 is 22.50 Å with a standard deviation of 0.19 Å, and minimum and maximum values of 21.06 Å and 23.34 Å.

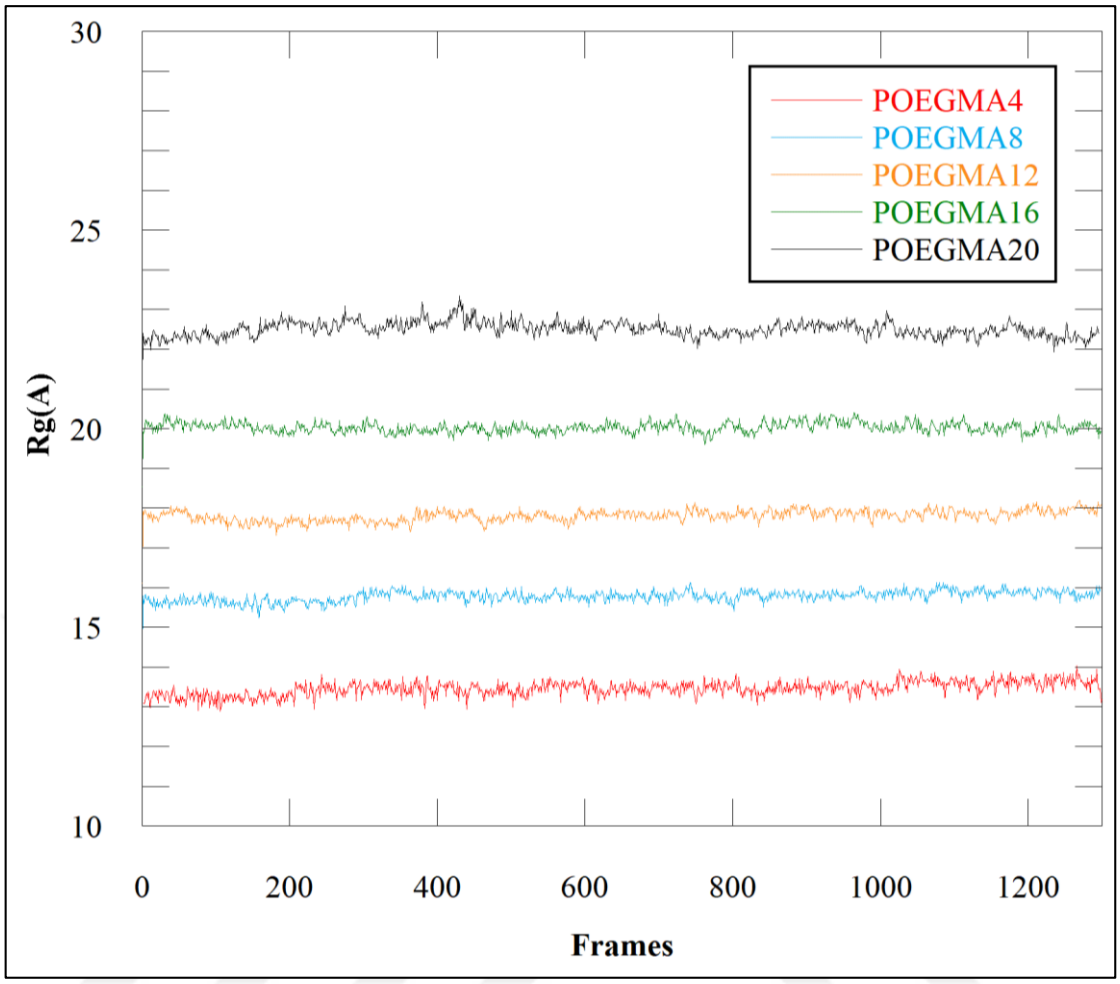

Figure 4.3 POEGMA -4, -8, -12, -16 and -20mers radius of gyration

The R_g analysis shows that even though PEG20 has a lower mean R_g value than POEGMA4, which has an equal number of EG monomers, POEGMA is much more stable with comparatively far less standard deviation, 1.61 Å for PEG20 compared to 0.18 Å for POEGMA4. The difference is much more pronounced in PEG40, and the R_g value is much more erratic compared to its POEGMA counter parts, with mean value of 13.41 Å but with a standard deviation of around 2.81 Å. On the other hand, even though the POEGMA8 has a larger mean value of 15.78 Å, but it is again much more stable, where the standard deviation is only 0.143. Even when compared with the POEGMA20, which has a standard deviation of around 0.27 Å, PEGs' has much more unstable R_g distribution while POEGMA has a more stable profile. Moreover, the change of R_g values for POEGMA is much more even and at a gradient as the chain size is increased, as when chain number are doubled from 4 to 8, the mean R_g value only changes by only 2.32 Å,

while for PEG, the when for the difference between R_g values of PEG20 and 40 is around 3.78 Å.

4.2. Watershell Analysis

The hydration behaviour of the polymer were analyzed by calculating the number of water molecule around the polymer chain. A cutoff radius of 5.0 Å was selected for the watershell calculation and the number of unique water molecules using the residue id of the fragments, the plot of the number of water molecules (N(H2O)) surrounding for the whole polymer within the cutoff distance for both PEG20 and PEG40 can be seen in Figure 4.4.

According to the results in Figure 4.4, the mean N(H2O) in the water shell surrounding the PEG20 polymer is 244.9 in each frame, with a standard deviation of 20.06 from the mean value. The lowest value was at the start of the simulation, where the H20 count was around 93, whereas the highest value was 293, which was around 800^{th} frame. On the other hand, PEG40 has the lowest N(H2O) molecules value at the start(154) to its highest value (542) at around 500^{th} frame which is 7.5 ns. The average N(H2O) in the watershell is around 418.6 in each frame with each standard deviation value of 50.13 water molecules from the mean. The watershell count around PEG20 compared to PEG40 is more stable. This fluctuating behavior in PEG40 watershell count coincides with R_g change through the course of the simulation.

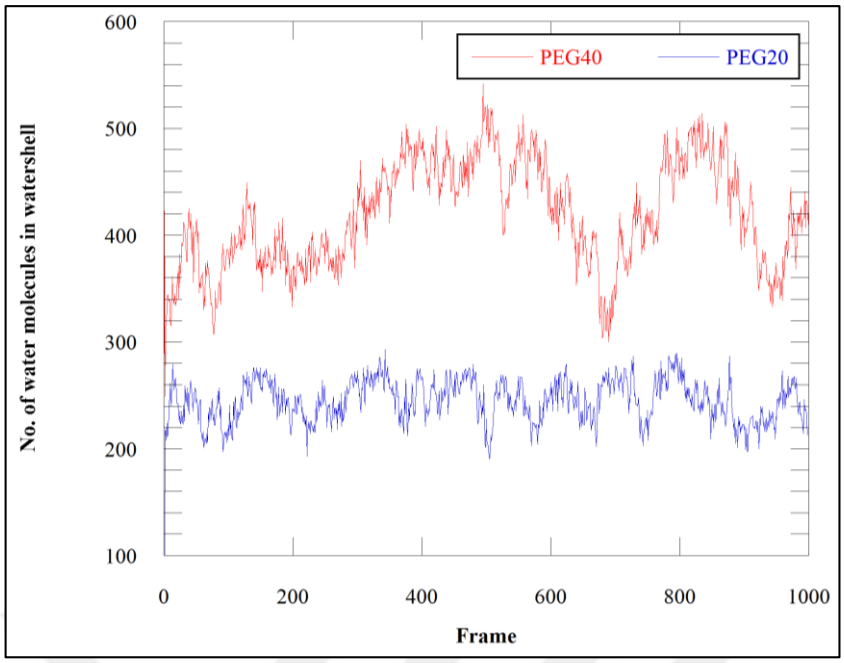

Figure 4.4 PEG20 and PEG40 watershell analysis

The watershell analysis graph of Figure 4.5 shows that POEGMA oligomers behave differently compared to PEG, the N(H2O) in watershell is much more stable. For the POEGMA polymers the mean N(H2O) within 5 Å distance of the polymer, in each frame throughout the simulation are 388.76, 741.05, 1106.5, 1448.1, and 1796.3 for the 4-, 8-, 12-, 16- and 20-mer POEGMA, respectively. From the watershell analysis graphs of individual POEGMA -mers in Appendix B, it can be seen that small trends in the data, similar to POEGMA4, 8-mers POEGMA has compact distribution of N(H2O) molecules around the mean value without sharp fluctuations because in both cases the backbone are not long, therefore the side chains are not crowded, as a result even at the solvent accessible surface area does not change significantly enough.

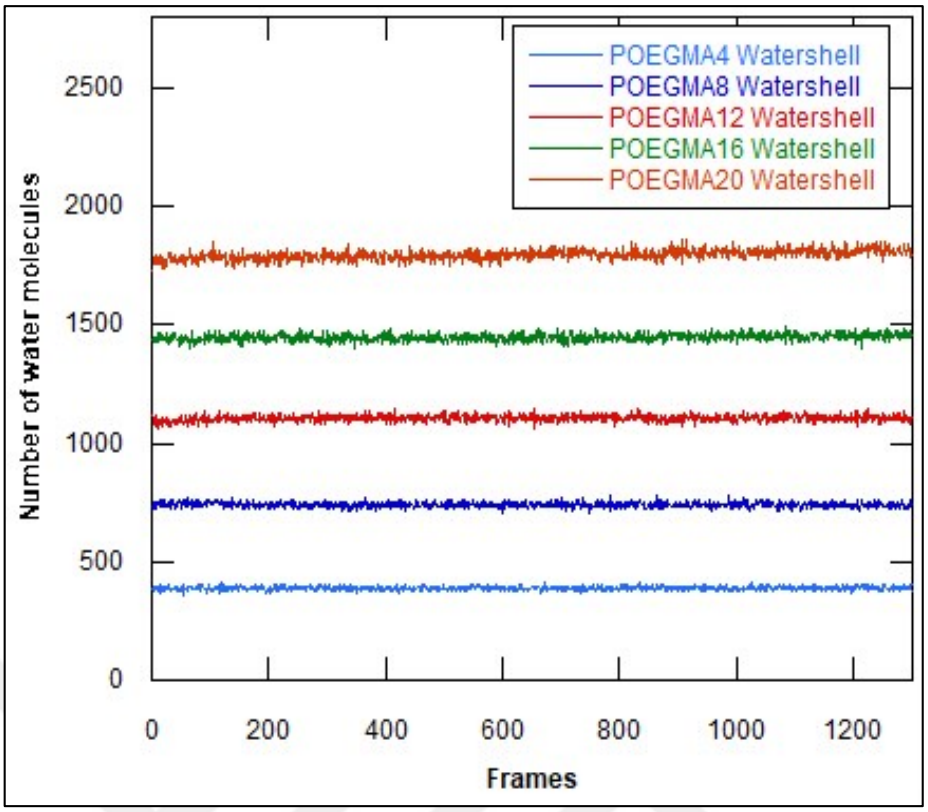

Figure 4.5 All POEGMA watershell analysis comparison

In the cases of POEGMA12, N(H2O) increases gradually till 200th frame, the average changing from 1090 to 1120, for 16-mer system, the N(H2O) in the watershell shows a very gradual increase from the start till the end and the 20-mer close analysis of watershell graph also shows an upward trend, the trend is much more steeper the 20-mer compared to increase in the 12- and 16-mer. This can be attributed to the hydration of the sidechain as the backbone curls and the polymer shape changes from comb to globular conformation as a result the sidechains which are in a closely packed at the start of the simulation spreads out as the backbone rolls up while spreading the side chains. The individual watershell analysis graphs for all polymer chains are in Appendix C.

4.3. Hydrogen Bonding Analysis

H-bonds between water and the polymer are vital in understanding the hydration dynamics. The water donor hydrogen atoms and polymer acceptor Oxygen atoms were

selected based on their atom type, the cutoff distance of 3.5 Å and cutoff angle of 135 degrees were designated.

In Figure 4.6, the left panel shows the hydrogen bond count per frame through the simulation of PEG20- and 40-mer chains in water system at 310 K. Both PEG chains show a consistent and H-bond per frame, the mean count per frame of the whole simulation for PEG20 is around 26.12 H-bonds with standard deviation of 2.98, while PEG40 has 50.1 H-bonds with standard deviation of 4.6, which is almost double of the PEG20 showing a direct relation between the chain length and the H-bond count.

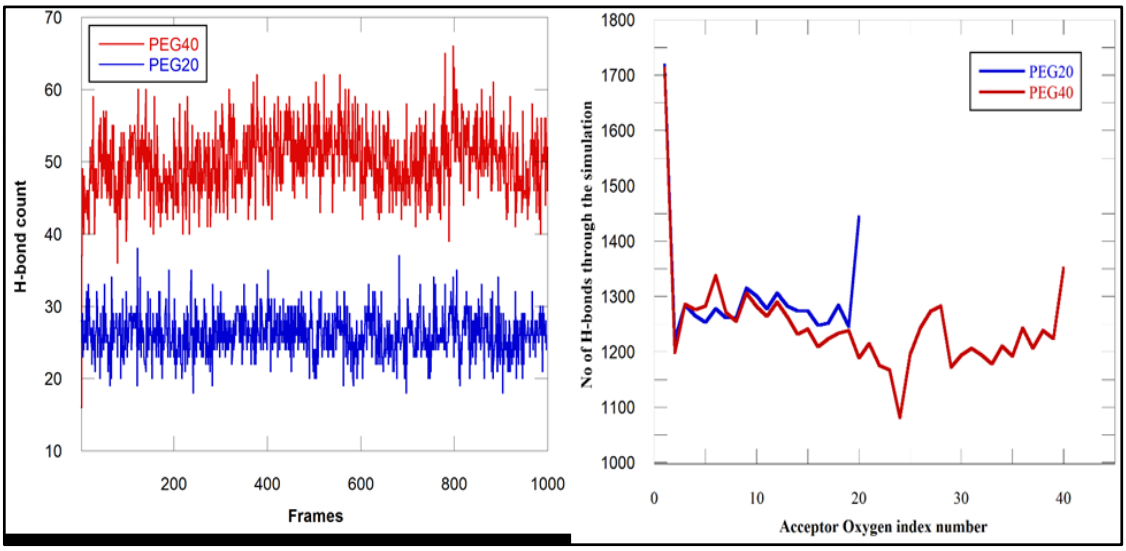

Figure 4.6 (Left) Hbond count of PEGs for each frame. (Right) PEG20, and PEG40 H-bond distribution for each oxygen in the polymer

The right panel of Figure 4.6 shows the number of hydrogen bonds involving each oxygen atom in the PEG chains. The plot shows that the oxygen atoms in the first and last monomeric units of the polymer are much more involved in the H-bond network around the polymer, which is understandable considering both are hydroxyl ends. For PEG40, a notable decrease in the hydrogen bond (H-bond) count is observed for oxygen atoms of monomeric units near the central region, particularly around the oxygen atom of 22nd monomeric unit. This phenomenon may be attributed to the fact that this oxygen atom is located at the center of a random coil structure, where it is less accessible water molecules for H-bond formation compared to oxygen atoms of the terminal monomer units of the chain. The central region of the coil is likely to experience greater steric constraints and reduced conformational flexibility, thereby limiting its participation in H-bonding

interactions relative to other oxygen atoms along the polymer backbone. The stability in the H-bond count for both PEG20 and 40 chains confirms its ability to maintain hydration level around the polymer, giving the molecule or drug attached to it a layer of protection against the surrounding environment, which is vital for biomaterial applications.

PEG chains exhibited a consistent and relatively high H-bond count per frame, reflecting the strong hydrogen-bonding capability of their ether oxygen atoms. The linear structure of PEG allows for efficient hydration, with water molecules forming stable hydrogen bonds along the polymer backbone.

The H-bond count per frame was also analyzed for POEGMA chains of 4-, 8-, 12-, 16-, and 20-mer with 5-OEG long side chains. The results are shown in Figure 4.7. It shows that the H-bond count per frame increases with an increase in the length of the polymer chains. As the number of OEG side chains is increased, there are more ethylene glycol units (hence -O-in the ether bond) available for H-bonding. For example, the mean H-bond count for POEGMA4 in each frame is around 20 while for POEGMA20 it is around 90 H-bonds per frame. The POEGMA 4 and 6 H-bond counts were comparatively stable through the entire simulation, but -12, -16 and -20mers POEGMA showed more variation over course of 15 ns simulation, this can be either due to the chain conformation not reaching stability or can be due to dynamic hydration of hydrophobic methacrylate backbone. The individual graphs for each polymer chain are given in Appendix C.

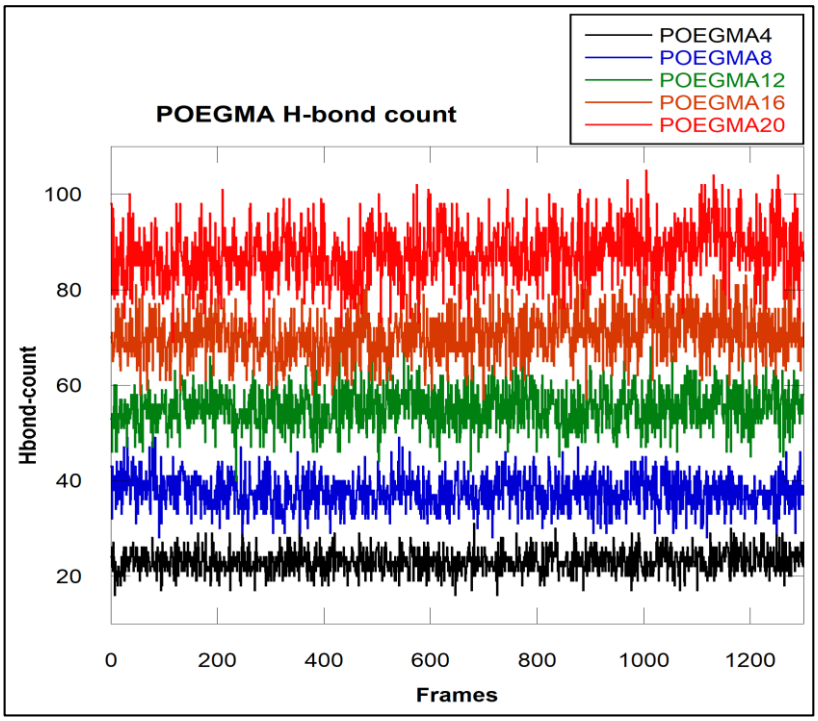

Figure 4.7 H-bond count for each frame for all POEGMA –mers.

In order to gain a better understanding of the hydration behaviour, a deeper look at the H-bond of each oxygen atom was taken and the results are provided in Figure 4.8. The first part of the graph comprising of graph in between two peaks in the hydrogen bond count gives us H-bond count for the oxygen atoms in the ester groups near backbone of POEGMA, while the latter portion of the data comprising of many smaller peaks describe the H-bond count of ethylene glycol sidechains.

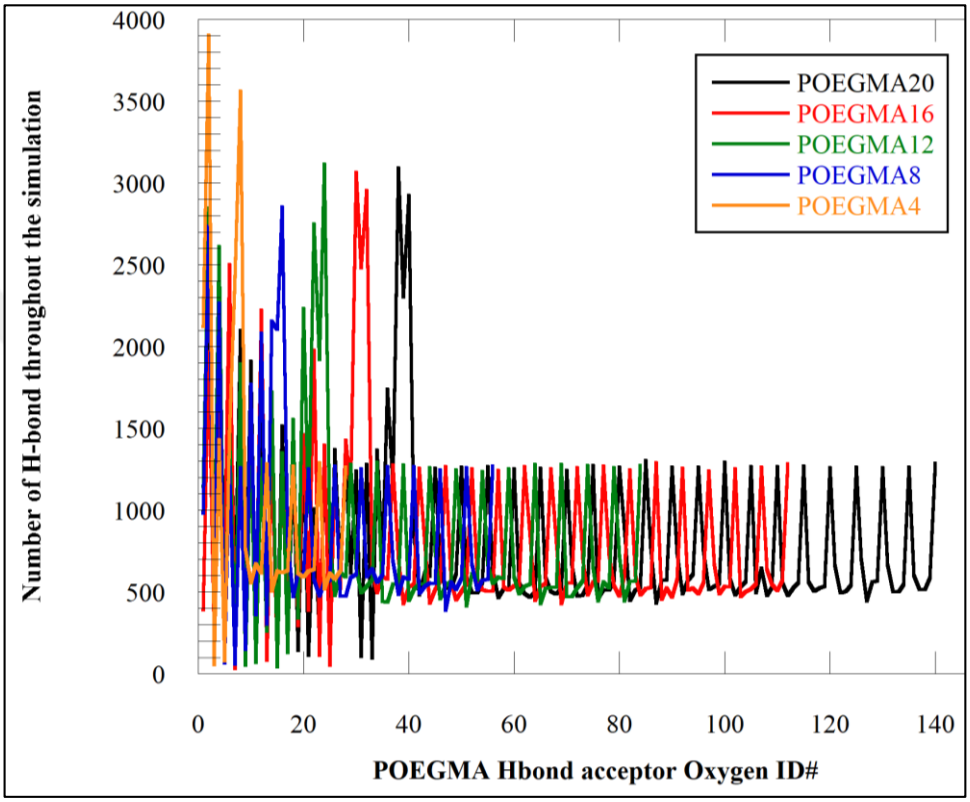

Figure 4.8 Number of H-bonds for each oxygen atom for the whole simulation

Figure 4.9 consists of five separate graphs for each of POEGMA -4, -8, -12, -16 and -20mers. In all graphs, it can be clearly seen that the oxygen atoms of ester group at the last monomeric units at both end of the polymeric chain forms the largest number of H-bonds, while the ester oxygen atoms in the middle of the backbone forms the least number of H-bonds throughout the simulation; the number progressively decreases toward the center from either side. This behavior can be due to the greater hydration level of the polymer termini, being at the ends of the POEGMA, these oxygen atoms are less packed and, therefore, more exposed to the surrounding water molecules, hence increasing their chance of making hydrogen bonds. On the other hand, the middle oxygen atoms are more packed together by the side chains and localized within the hydrophobic

core of the methacrylate backbone reducing their accessibility by water molecules, as a result their ability to form H-bonds with water molecules is decreased.

The graphs in Figure 4.9 also show a distinct behavior of the OEG side chain oxygen atoms. In the second part of graphs, it can be observed that the number of small peaks equal to the number of the OEG side chains and the terminal OEG side chain oxygen atoms are responsible for peak H-bond counts on all the branches. This is mainly due to the locations of the acceptor atoms, allowing them to interact freely with water molecules with less steric hindrance. This high H-bond count shows their role in hydration shell stabilization around the polymer. The H-bond counts decrease for the oxygen atoms that are closer to the backbone. This change is mainly due to the growing steric hindrance and the reduced water molecule accessibility.

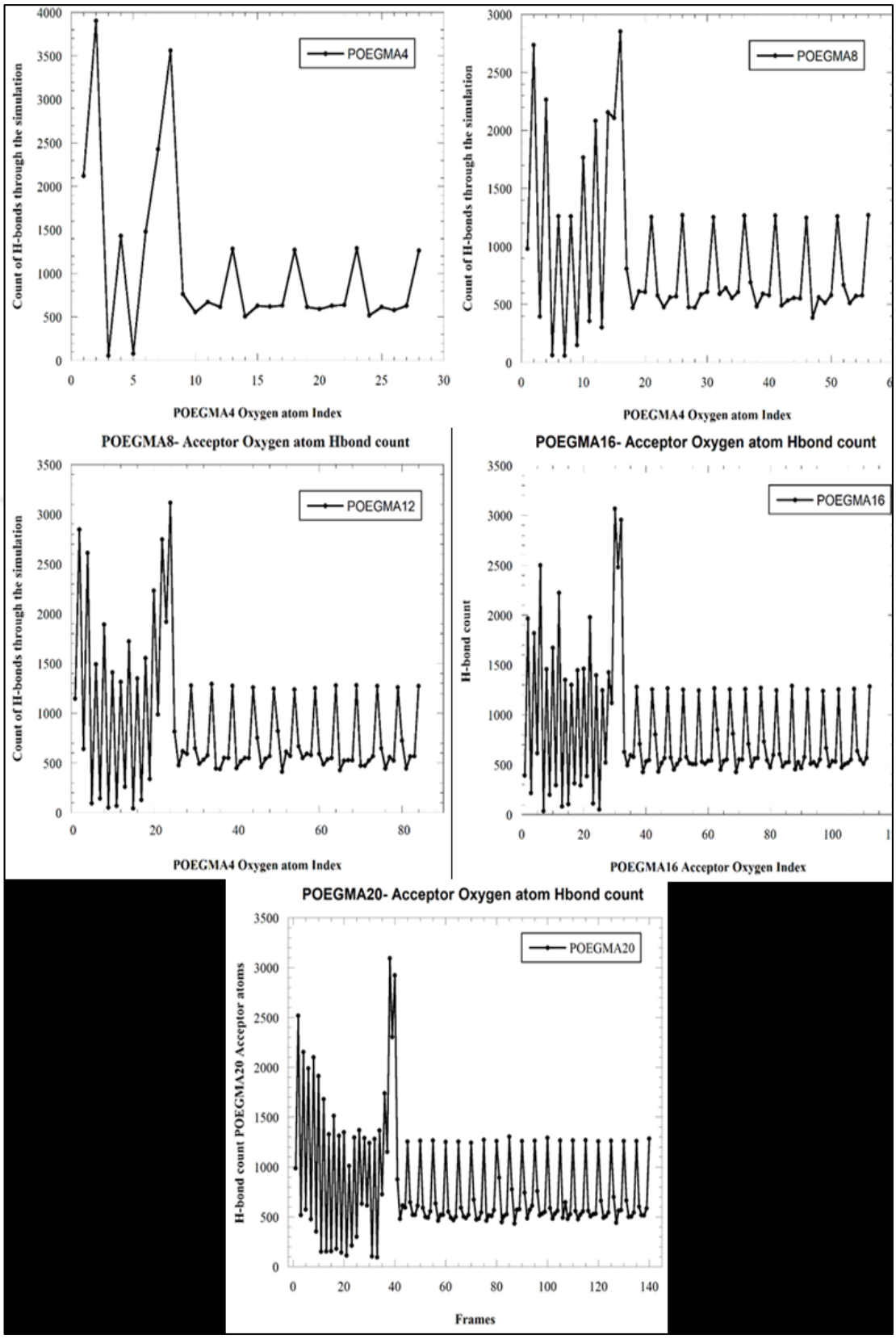

Figure 4.9 H-bond count distribution for -4, -8, -12, -16 and -20mers POEGMA Oxygen atoms

Figure 4.6 for PEG20 and 40 shows H-bond counts for each oxygen atom, where the terminus oxygen atoms have higher H-bond counts due to reduced hindrance and increased accessibility to hydration shell. On the other hand, for central ethylene glycol units of PEG chains, similar to POEGMA chains H-bond counts were reduced mainly due to increased hindrance and reduced water molecule accessibility.

For both PEG20 and PEG40 the H-bond behavior aligns with the radius of gyration and the watershell analysis of the respective chain. The stability of H-bond counts for PEG polymer chains shows its ability to maintain its hydration level. For PEG20 we can see in Figure 4.11 that the R_g is comparatively stable compared to PEG40 even though the value is changing. When it is compared to the watershell analysis graph there is similar trends, and this pattern further aligns with H-bond analysis, where the small changes align with the change in N(H2O) in the watershell, which is further supported by the R_g distribution. Moreover, for PEG40, the peaks and valleys in both R_g and watershell analysis are similar, which is further translated in H-bond analysis but a little less pronounced.

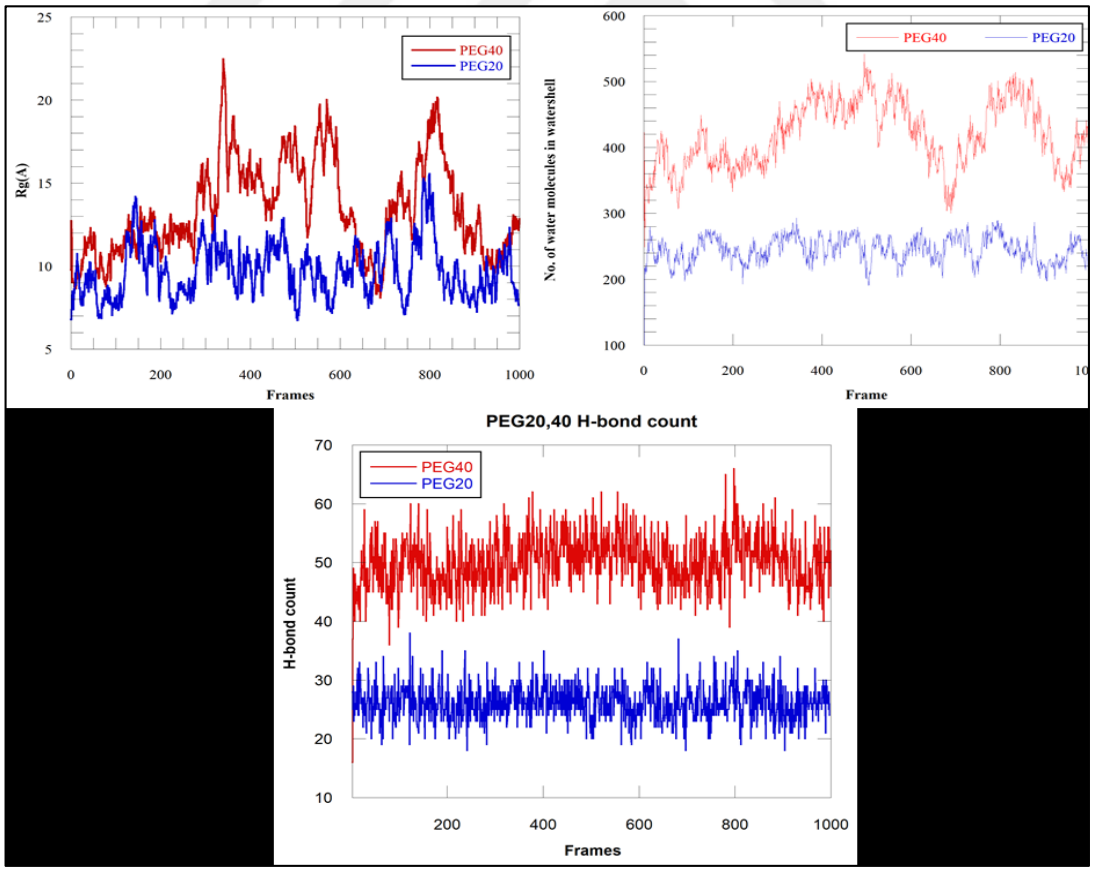

Figure 4.10 PEG20 and PEG40 Rg analysis (top left), Watershell analysis (top right) and H-bond analysis (bottom) graphs

For POEGMA, the H-bond count distribution also aligns with R_g analysis. The R_g values of POEGMA chains indicate that they form a packed conformation with the hydrophilic OEG side chains spreading out and shielding the methacrylate hydrophobic core from the solvents molecules. In the larger POEGMA polymers, it is observed that the polymer is curling up with the backbone in the center forming almost globular chain, as a result acceptor oxygen atoms of monomeric units in center of the polymer are less hydrated while the oxygen atoms in the terminal monomeric units are more exposed to the hydration shell to interact. Furthermore, ester oxygen atoms in both terminal monomeric units near ends of the backbone and the oxygen atoms at last ethylene units of the side chains have high H-bond count, suggesting that these regions are significant for the stability of the watershell around the polymer. On the other hand, the low H-bond count of oxygen atom near the hydrophobic core indicated a lower hydration level of those regions. These characteristics align with the compact conformation of all POEGMA chains indicated by its R_g values. The snapshots of MD simulation are given in Appendix B.

The observed behaviour of POEGMA form R_g, watershell and H-bond analysis shows that it has the capability to form gradient of H-bonds with side chains well hydrated compared to its backbone, which gives control of its hydration properties. Furthermore, high H-bonding ability of oxygen atoms located at the side chain end ensures a stable watershell evident from the watershell analysis, which is necessary for non-fouling characteristics and preventing non-specific adsorption while enhancing biocompatibility of pharmaceutical products. Furthermore, the hydrophobic backbone with far less hydration and H-bond count of core oxygen gives it structural stability.

CHAPTER 5

CONCLUSIONS AND RECOMMENDATIONS

This section covers the study's overview and conclusion, as well as its limits, suggestions, and future directions.

5.1. Conclusions

This research aimed to investigate and compare the interactions of PEG and POEGMA with water using MD simulations. The study started by creating molecular models for single polymers, i.e. PEG having 20- and 40-repeating units and POEGMA of 4-, 8-, 12-, 16- and 20- repeating units solvated in cubic water boxes were made using CHARMM GUI[95] and Avogadro[96]. TRUBA[111] high-performance computing platform was used to perform MD simulations using LAMMPS software[101]. The subsequent simulation results in form dcd trajectories were reorganized and analyzed using VMD[106] and MDAnalysis[107]. Three key properties, such as the radius of gyration (R_g), watershell, and hydrogen bond (H-bond) analysis, were performed to compare how the two polymers interact with water.

R_g values of PEG were lower but less reflecting its ability to form compact and flexible helical random coil structures in aqueous environment. In contrast, R_g values for shorter POEGMA chains were slightly higher, due to its short hydrophilic chains and hydrophobic backbone, while as the length of the polymer chain grew, the change in R_g values was small as the longer chains started to form a globular structure. Watershell analysis showed that N(H2O) around the PEG was not stable mainly due to the unstable conformation, while POEGMA showed more stable and higher N(H2O) in the watershell which was mainly due to its expanded and well hydrated side chains. PEG exhibited higher H-bond counts, and its terminal oxygen atoms forming the most number of H-bonds through the entire simulation while the oxygen atom at the center of the polymer contributed the least. On the other hand, for POEGMA, the H-bond counts were slightly lower compared to equivalent PEG polymers. Among all oxygen atoms in the polymer, the oxygen atom of ester group of the terminal monomeric unit end form the highest

number of H-bonds while among the oxygen atoms of the central units' ester groups contribute the least. The oxygen H-bond counts also decrease as we move from the end of the side chains toward the backbone.

In short, the hydrophilic nature of PEG results in compact random coil conformation with helical regions, with slightly less stable watershell but high H-bond counts. On the other hand POEGMA exhibits more tunable behavior, i.e. R_g values, water shell and H-bonds are stable and changing on a gradient with polymer's chain length, making it ideal for applications requiring controlled interactions with water.

5.2. Recommendations and Future Directions

Future studies could perform simulations which have PEG of longer chain lengths. Moreover, simulations with longer production can also be performed ensuring, proper stabilization of longer polymer chains. The effect of side chain length and architecture on the properties of POEGMA can also be investigated. Furthermore, there can be comparison of interaction of PEG and POEGMA with different protein or phospholipid bilayer systems. In addition to these, there can be experimental results to compliment the simulation results.

REFERENCES

1. Bailey, F. E.; Koleske, J. V. Poly(Ethylene Oxide); *Academic Press: New York*, **1976**, 1 (3), 1-4. https://doi.org/10.1016/B978-0-12-073250-0.X5001-6.
2. Albertsson, P. Å. Partition of Cell Particles and Macromolecules : Separation and Purification of Biomolecules, Cell Organelles, Membranes, and Cells in Aqueous Polymer Two-Phase Systems and Their Use in Biochemical Analysis and Biotechnology; *New York : Wiley*, **1986**, 346, https://doi.org/10.1002/cbf.290050311.
3. Kao, K. N.; Constabel, F.; Michayluk, M. R.; Gamborg, O. L. Plant Protoplast Fusion and Growth of Intergeneric Hybrid Cells. *Planta* **1974**, 120 (3), 215–227. https://doi.org/10.1007/BF00390290.
4. Ahkong, Q. F.; Fisher, D.; Tampion, W.; Lucy, J. A. Mechanisms of Cell Fusion. *Nature* **1975**, 253 (5488), 194–195. https://doi.org/10.1038/253194a0.
5. Pontecorvo, G. Production of Mammalian Somatic Cell Hybrids by Means of Polyethylene Glycol Treatment. Somatic Cell. *Genet* **1975**, 1 (4), 397–400. https://doi.org/10.1007/BF01538671.
6. Harris, J. M.; Case, M. G. Poly(Ethylene Glycol) Ethers as Recoverable Phase-Transfer Agents in Permanganate Oxidations. *J. Org. Chem.* **1983**, 48 (26), 5390–5392. https://doi.org/10.1021/jo00174a057.
7. Bailey, F. E.; Koleske, J. V. Alkylene Oxides and Their Polymers; Taylor & Francis: *Boca Raton*, **1991**, 272, https://doi.org/10.1201/9781003066569.
8. Dust, J. M.; Fang, Z. H.; Harris, J. M. Proton NMR Characterization of Poly(Ethylene Glycols) and Derivatives. *Macromolecules* **1990**, 23 (16), 3742–3746. https://doi.org/10.1021/ma00218a005.
9. Poly(Ethylene Glycol): Chemistry and Biological Applications; Harris, J. M., Zalipsky, S., American Chemical Society, Eds.; ACS symposium series; *American Chemical Society: Washington, DC*, **1997**. https://doi.org/10.1021/bk-1997-0680.
10. Harris, J. M.; Chess, R. B. Effect of Pegylation on Pharmaceuticals. *Nat. Rev. Drug Discov.* **2003**, 2 (3), 214–221. https://doi.org/10.1038/nrd1033.
11. Suk, J. S.; Xu, Q.; Kim, N.; Hanes, J.; Ensign, L. M. PEGylation as a Strategy for Improving Nanoparticle-Based Drug and Gene Delivery. *Adv. Drug Deliv. Rev.* **2016**, 99, 28–51. https://doi.org/10.1016/j.addr.2015.09.012.
12. Polson, A.; Potgieter, G. M.; Largier, J. F.; Mears, G. E.; Joubert, F. J. THE FRACTIONATION OF PROTEIN MIXTURES BY LINEAR POLYMERS OF HIGH MOLECULAR WEIGHT. *Biochim. Biophys. Acta* **1964**, 82, 463–475. https://doi.org/10.1016/0304-4165(64)90438-6.
13. Chun, P. W.; Fried, M.; Ellis, E. F. Use of Water-Soluble Polymers for the Isolation and Purification of Human Immunoglobulins. *Anal. Biochem.* **1967**, 19 (3), 481–497. https://doi.org/10.1016/0003-2697(67)90239-4.
14. Sim, S.-L.; He, T.; Tscheliessnig, A.; Mueller, M.; Tan, R. B. H.; Jungbauer, A. Protein Precipitation by Polyethylene Glycol: A Generalized Model Based on Hydrodynamic Radius. *J. Biotechnol.* **2012**, 157 (2), 315–319. https://doi.org/10.1016/j.jbiotec.2011.09.028.

15. Veronese, F. M.; Pasut, G. PEGylation, Successful Approach to Drug Delivery. *Drug Discov. Today* **2005**, 10 (21), 1451–1458. https://doi.org/10.1016/S1359-6446(05)03575-0.
16. Abuchowski, A.; van Es, T.; Palczuk, N. C.; Davis, F. F. Alteration of Immunological Properties of Bovine Serum Albumin by Covalent Attachment of Polyethylene Glycol. *J. Biol. Chem.* **1977**, 252 (11), 3578–3581.
17. Allen, T. M.; Cullis, P. R. Liposomal Drug Delivery Systems: From Concept to Clinical Applications. *Adv. Drug Deliv. Rev.* **2013**, 65 (1), 36–48. https://doi.org/10.1016/j.addr.2012.09.037.
18. Liu, Z.; Robinson, J. T.; Sun, X.; Dai, H. PEGylated Nanographene Oxide for Delivery of Water-Insoluble Cancer Drugs. *J. Am. Chem. Soc.* **2008**, 130 (33), 10876–10877. https://doi.org/10.1021/ja803688x.
19. Mori, Y.; Nagaoka, S.; Takiuchi, H.; Kikuchi, T.; Noguchi, N.; Tanzawa, H.; Noishiki, Y. A New Antithrombogenic Material with Long Polyethyleneoxide Chains. Trans. - *Am. Soc. Artif. Intern. Organs* **1982**, 28, 459–463.
20. Tirosh, O.; Barenholz, Y.; Katzhendler, J.; Priev, A. Hydration of Polyethylene Glycol-Grafted Liposomes. *Biophys. J.* **1998**, 74 (3), 1371–1379. https://doi.org/10.1016/S0006-3495(98)77849-X.
21. Branca, C.; Magazù, S.; Maisano, G.; Migliardo, F.; Migliardo, P.; Romeo, G. Hydration Study of PEG/Water Mixtures by Quasi Elastic Light Scattering, Acoustic and Rheological Measurements. *J. Phys. Chem. B* **2002**, 106 (39), 10272–10276. https://doi.org/10.1021/jp014345v.
22. Jeon, S. I., J. H. Lee, J. D. Andrade, and PrG De Gennes. Protein—Surface Interactions in the Presence of Polyethylene Oxide: I. Simplified Theory. *J. Colloid Interface Sci.* **1991**, 142 (1), 149–158.
23. Needham, D.; McIntosh, T. J.; Lasic, D. D. Repulsive Interactions and Mechanical Stability of Polymer-Grafted Lipid Membranes. Biochim. *Biophys. Acta* **1992**, 1108 (1), 40–48. https://doi.org/10.1016/0005-2736(92)90112-y.
24. Yang, Q.; Lai, S. K. Anti-PEG Immunity: Emergence, Characteristics, and Unaddressed Questions. Wiley Interdiscip. *Rev. Nanomed. Nanobiotechnol.* **2015**, 7 (5), 655–677. https://doi.org/10.1002/wnan.1339.
25. Vonarbourg, A.; Passirani, C.; Saulnier, P.; Benoit, J.-P. Parameters Influencing the Stealthiness of Colloidal Drug Delivery Systems. *Biomaterials* **2006**, 27 (24), 4356–4373. https://doi.org/10.1016/j.biomaterials.2006.03.039.
26. Damodaran, V. B.; Fee, C. J.; Ruckh, T.; Popat, K. C. Conformational Studies of Covalently Grafted Poly(Ethylene Glycol) on Modified Solid Matrices Using X-Ray Photoelectron Spectroscopy. *Langmuir ACS J. Surf. Colloids* **2010**, 26 (10), 7299–7306. https://doi.org/10.1021/la9041502.
27. Jokerst, J. V.; Lobovkina, T.; Zare, R. N.; Gambhir, S. S. Nanoparticle PEGylation for Imaging and Therapy. *Nanomed.* **2011**, 6 (4), 715–728. https://doi.org/10.2217/nnm.11.19.
28. Dams, E. T.; Laverman, P.; Oyen, W. J.; Storm, G.; Scherphof, G. L.; van Der Meer, J. W.; Corstens, F. H.; Boerman, O. C. Accelerated Blood Clearance and Altered Biodistribution of Repeated Injections of Sterically Stabilized Liposomes. *J. Pharmacol. Exp. Ther.* **2000**, 292 (3), 1071–1079.
29. Wang, X.; Ishida, T.; Kiwada, H. Anti-PEG IgM Elicited by Injection of Liposomes Is Involved in the Enhanced Blood Clearance of a Subsequent Dose of PEGylated Liposomes. *J. Controlled Release* **2007**, 119 (2), 236–244. https://doi.org/10.1016/j.jconrel.2007.02.010.

30. Abu Lila, A. S.; Kiwada, H.; Ishida, T. The Accelerated Blood Clearance (ABC) Phenomenon: Clinical Challenge and Approaches to Manage. *J. Controlled Release* **2013**, 172 (1), 38–47. https://doi.org/10.1016/j.jconrel.2013.07.026.
31. Zhang, P.; Sun, F.; Liu, S.; Jiang, S. Anti-PEG Antibodies in the Clinic: Current Issues and beyond PEGylation. *J. Control. Release Off. J. Control. Release Soc.* **2016**, 244 (Pt B), 184–193. https://doi.org/10.1016/j.jconrel.2016.06.040.
32. Henry, C. E.; Wang, Y.-Y.; Yang, Q.; Hoang, T.; Chattopadhyay, S.; Hoen, T.; Ensign, L. M.; Nunn, K. L.; Schroeder, H.; McCallen, J.; Moench, T.; Cone, R.; Roffler, S. R.; Lai, S. K. Anti-PEG Antibodies Alter the Mobility and Biodistribution of Densely PEGylated Nanoparticles in Mucus. *Acta Biomater.* **2016**, 43, 61–70. https://doi.org/10.1016/j.actbio.2016.07.019.
33. Garay, R. P.; El-Gewely, R.; Armstrong, J. K.; Garratty, G.; Richette, P. Antibodies against Polyethylene Glycol in Healthy Subjects and in Patients Treated with PEG-Conjugated Agents. *Expert Opin. Drug Deliv.* **2012**, 9 (11), 1319–1323. https://doi.org/10.1517/17425247.2012.720969.
34. Cox, F.; Khalib, K.; Conlon, N. PEG That Reaction: A Case Series of Allergy to Polyethylene Glycol. J. *Clin. Pharmacol.* **2021**, 61 (6), 832–835. https://doi.org/10.1002/jcph.1824.
35. Hoang Thi, T. T.; Pilkington, E. H.; Nguyen, D. H.; Lee, J. S.; Park, K. D.; Truong, N. P. The Importance of Poly(Ethylene Glycol) Alternatives for Overcoming PEG Immunogenicity in Drug Delivery and Bioconjugation. *Polymers* **2020**, 12 (2), 298. https://doi.org/10.3390/polym12020298.
36. Stadler, V.; Kirmse, R.; Beyer, M.; Breitling, F.; Ludwig, T.; Bischoff, F. R. PEGMA/MMA Copolymer Graftings: Generation, Protein Resistance, and a Hydrophobic Domain. *Langmuir ACS J. Surf. Colloids* **2008**, 24 (15), 8151–8157. https://doi.org/10.1021/la800772m.
37. York, A. W.; Kirkland, S. E.; McCormick, C. L. Advances in the Synthesis of Amphiphilic Block Copolymers via RAFT Polymerization: Stimuli-Responsive Drug and Gene Delivery. *Adv. Drug Deliv. Rev.* **2008**, 60 (9), 1018–1036. https://doi.org/10.1016/j.addr.2008.02.006.
38. Lutz, J.-F.; Akdemir, Ö.; Hoth, A. Point by Point Comparison of Two Thermosensitive Polymers Exhibiting a Similar LCST: Is the Age of Poly(NIPAM) Over? *J. Am. Chem. Soc.* **2006**, 128 (40), 13046–13047. https://doi.org/10.1021/ja065324n.
39. Lutz, J.-F.; Andrieu, J.; Üzgün, S.; Rudolph, C.; Agarwal, S. Biocompatible, Thermoresponsive, and Biodegradable: Simple Preparation of "All-in-One" Biorelevant Polymers. *Macromolecules* **2007**, 40 (24), 8540–8543. https://doi.org/10.1021/ma7021474.
40. Lutz, J. Polymerization of Oligo(Ethylene Glycol) (Meth)Acrylates: Toward New Generations of Smart Biocompatible Materials. *J. Polym. Sci. Part Polym. Chem.* **2008**, 46 (11), 3459–3470. https://doi.org/10.1002/pola.22706.
41. Liu, M.; Leroux, J.-C.; Gauthier, M. A. Conformation–Function Relationships for the Comb-Shaped Polymer pOEGMA. *Prog. Polym. Sci.* **2015**, 48, 111–121. https://doi.org/10.1016/j.progpolymsci.2015.03.001.
42. Lee, H.; Lee, E.; Kim, D. K.; Jang, N. K.; Jeong, Y. Y.; Jon, S. Antibiofouling Polymer-Coated Superparamagnetic Iron Oxide Nanoparticles as Potential Magnetic Resonance Contrast Agents for in Vivo Cancer Imaging. *J. Am. Chem. Soc.* **2006**, 128 (22), 7383–7389. https://doi.org/10.1021/ja061529k.
43. Kim, D.; Park, S.; Lee, J. H.; Jeong, Y. Y.; Jon, S. Antibiofouling Polymer-Coated Gold Nanoparticles as a Contrast Agent for in Vivo X-Ray Computed Tomography

Imaging. *J. Am. Chem. Soc.* **2007**, 129 (24), 7661–7665. https://doi.org/10.1021/ja071471p.
44. Boyer, C.; Liu, J.; Wong, L.; Tippett, M.; Bulmus, V.; Davis, T. P. Stability and Utility of Pyridyl Disulfide Functionality in RAFT and Conventional Radical Polymerizations. *J. Polym. Sci. Part Polym. Chem.* **2008**, 46 (21), 7207–7224. https://doi.org/10.1002/pola.23028.
45. Boyer, C.; Bulmus, V.; Davis, T. P.; Ladmiral, V.; Liu, J.; Perrier, S. Bioapplications of RAFT Polymerization. *Chem. Rev.* **2009**, 109 (11), 5402–5436. https://doi.org/10.1021/cr9001403.
46. Boyer, C.; Liu, J.; Bulmus, V.; Davis, T. P. RAFT Polymer End-Group Modification and Chain Coupling/Conjugation Via Disulfide Bonds. *Aust. J. Chem*. **2009**, 62 (8), 830. https://doi.org/10.1071/CH09062.
47. Boyer, C.; Whittaker, M. R.; Chuah, K.; Liu, J.; Davis, T. P. Modulation of the Surface Charge on Polymer-Stabilized Gold Nanoparticles by the Application of an External Stimulus. *Langmuir ACS J. Surf. Colloids* **2010**, 26 (4), 2721–2730. https://doi.org/10.1021/la902746v.
48. Dalgakiran, E.; Tatlipinar, H. The Role of Hydrophobic Hydration in the LCST Behaviour of POEGMA300 by All-Atom Molecular Dynamics Simulations. *Phys. Chem. Chem. Phys.* **2018**, 20 (22), 15389–15399. https://doi.org/10.1039/C8CP02026D.
49. Xu, F.; Dawson, C.; Hoare, T. Multicellular Layered Nanofibrous Poly(Oligo Ethylene Glycol Methacrylate) (POEGMA)-Based Hydrogel Scaffolds via Reactive Cell Electrospinning. *Adv. Biol.* **2023**, 7 (10), 2300052. https://doi.org/10.1002/adbi.202300052.
50. Sano, K.; Umemoto, K.; Miura, H.; Ohno, S.; Iwata, K.; Kawakami, R.; Munekane, M.; Yamasaki, T.; Citterio, D.; Hiruta, Y.; Mukai, T. Feasibility of Using Poly[Oligo(Ethylene Glycol) Methyl Ether Methacrylate] as Tumor-Targeted Carriers of Diagnostic Drugs. *ACS Appl. Polym. Mater. 2022*, 4 (7), 4734–4740. https://doi.org/10.1021/acsapm.2c00312.
51. Fermi, E.; Pasta, P.; Ulam, S.; Tsingou, M. STUDIES OF THE NONLINEAR PROBLEMS; *LA-1940, 4376203*; **1955**; p LA-1940, 4376203. https://doi.org/10.2172/4376203.
52. Brooks, C. L. Computer Simulation of Liquids. *J. Solut. Chem*. **1989**, 18 (1), 99–99. https://doi.org/10.1007/BF00646086.
53. Frenkel, D.; Smit, B. Understanding Molecular Simulation : *From Algorithms to Applications. 2nd Ed.*; **2002**, 4 (12), 63-107, https://doi.org/10.1016/B978-0-12-267351-1.X5000-7
54. Paquet, E.; Viktor, H. L. Molecular Dynamics, Monte Carlo Simulations, and Langevin Dynamics: A Computational Review. *BioMed Res. Int. 2015*, **2015**, 183918. https://doi.org/10.1155/2015/183918.
55. Alder, B. J.; Wainwright, T. E. Phase Transition for a Hard Sphere System. J. *Chem. Phys.* **1957**, 27 (5), 1208–1209. https://doi.org/10.1063/1.1743957.
56. Rahman, A. Correlations in the Motion of Atoms in Liquid Argon. *Phys. Rev.* **1964**, 136 (2A), A405–A411. https://doi.org/10.1103/PhysRev.136.A405.
57. Adcock, S. A.; McCammon, J. A. Molecular Dynamics: Survey of Methods for Simulating the Activity of Proteins. *Chem. Rev.* **2006**, 106 (5), 1589. https://doi.org/10.1021/cr040426m.
58. Rahman, A.; Stillinger, F. H. Molecular Dynamics Study of Liquid Water. *J. Chem. Phys.* **1971**, 55 (7), 3336–3359. https://doi.org/10.1063/1.1676585.

59. Stillinger, F. H.; Rahman, A. Molecular Dynamics Study of Temperature Effects on Water Structure and Kinetics. *J. Chem. Phys.* **1972**, 57 (3), 1281–1292. https://doi.org/10.1063/1.1678388.
60. Stillinger, F. H.; Rahman, A. Improved Simulation of Liquid Water by Molecular Dynamics. *J. Chem. Phys*. **1974**, 60 (4), 1545–1557. https://doi.org/10.1063/1.1681229.
61. McCammon, J. A.; Gelin, B. R.; Karplus, M. Dynamics of Folded Proteins. *Nature* **1977**, 267 (5612), 585–590. https://doi.org/10.1038/267585a0.
62. Chmiela, S.; Sauceda, H. E.; Müller, K.-R.; Tkatchenko, A. Towards Exact Molecular Dynamics Simulations with Machine-Learned Force Fields. *Nat. Commun. 2018*, 9 (1), 3887. https://doi.org/10.1038/s41467-018-06169-2.
63. Karplus, M.; McCammon, J. A. Molecular Dynamics Simulations of Biomolecules. *Nat. Struct. Biol.* **2002**, 9 (9), 646–652. https://doi.org/10.1038/nsb0902-646.
64. Hollingsworth, S. A.; Dror, R. O. Molecular Dynamics Simulation for All. *Neuron* **2018**, 99 (6), 1129–1143. https://doi.org/10.1016/j.neuron.2018.08.011.
65. Hairer, E.; Lubich, C.; Wanner, G. Geometric Numerical Integration Illustrated by the Störmer–Verlet Method. *Acta Numer.* **2003**, 12, 399–450. https://doi.org/10.1017/S0962492902000144.
66. Gunsteren, W. F. V.; Berendsen, H. J. C. A Leap-Frog Algorithm for Stochastic Dynamics. *Mol. Simul.* **1988**. https://doi.org/10.1080/08927028808080941.
67. Leckband, D.; Israelachvili, J. Intermolecular Forces in Biology. *Q. Rev. Biophys.* **2001**, 34 (2), 105–267. https://doi.org/10.1017/S0033583501003687.
68. Hospital, A.; Goñi, J. R.; Orozco, M.; Gelpí, J. L. Molecular Dynamics Simulations: Advances and Applications. *Adv. Appl. Bioinforma. Chem. AABC* **2015**, 8, 37. https://doi.org/10.2147/AABC.S70333.
69. MacKerell, A. D.; Bashford, D.; Bellott, M.; Dunbrack, R. L.; Evanseck, J. D.; Field, M. J.; Fischer, S.; Gao, J.; Guo, H.; Ha, S.; Joseph-McCarthy, D.; Kuchnir, L.; Kuczera, K.; Lau, F. T. K.; Mattos, C.; Michnick, S.; Ngo, T.; Nguyen, D. T.; Prodhom, B.; Reiher, W. E.; Roux, B.; Schlenkrich, M.; Smith, J. C.; Stote, R.; Straub, J.; Watanabe, M.; Wiórkiewicz-Kuczera, J.; Yin, D.; Karplus, M. All-Atom Empirical Potential for Molecular Modeling and Dynamics Studies of Proteins. *J. Phys. Chem. B* **1998**, 102 (18), 3586–3616. https://doi.org/10.1021/jp973084f.
70. Cornell, W. D.; Cieplak, P.; Bayly, C. I.; Gould, I. R.; Merz, K. M.; Ferguson, D. M.; Spellmeyer, D. C.; Fox, T.; Caldwell, J. W.; Kollman, P. A. A Second Generation Force Field for the Simulation of Proteins, Nucleic Acids, and Organic Molecules. *J. Am. Chem. Soc.* **1995**, 117 (19), 5179–5197. https://doi.org/10.1021/ja00124a002.
71. The OPLS [optimized potentials for liquid simulations] potential functions for proteins, energy minimizations for crystals of cyclic peptides and crambin | *Journal of the American Chemical Society.* **1988**, https://pubs.acs.org/doi/abs/10.1021/ja00214a001
72. GROMOS Force Field - van Gunsteren - *Major Reference Works - Wiley Online Library,* **1998,** https://onlinelibrary.wiley.com/doi/10.1002/0470845015.cga011 (accessed 2025-03-04).
73. Merck molecular force field. I. Basis, form, scope, parameterization, and performance of MMFF94 - Halgren - *Journal of Computational Chemistry - Wiley Online Library.* **1996,** https://onlinelibrary.wiley.com/doi/10.1002/(SICI)1096-987X(199604)17:5/6%3C490::AID-JCC1%3E3.0.CO;2-P (accessed 2025-03-04).
74. Heid, E.; Fleck, M.; Chatterjee, P.; Schröder, C.; MacKerell, A. D. Jr. Toward Prediction of Electrostatic Parameters for Force Fields That Explicitly Treat Electronic Polarization. *J. Chem. Theory Comput.* **2019**, 15 (4), 2460–2469. https://doi.org/10.1021/acs.jctc.8b01289.

75. Ganson, N. J.; Kelly, S. J.; Scarlett, E.; Sundy, J. S.; Hershfield, M. S. Control of Hyperuricemia in Subjects with Refractory Gout, and Induction of Antibody against Poly(Ethylene Glycol) (PEG), in a Phase I Trial of Subcutaneous PEGylated Urate Oxidase. *Arthritis Res. Ther.* **2006**, 8 (1), R12. https://doi.org/10.1186/ar1861.
76. Sherman, M. R.; Saifer, M. G. P.; Perez-Ruiz, F. PEG-Uricase in the Management of Treatment-Resistant Gout and Hyperuricemia. *Adv. Drug Deliv. Rev.* **2008**, 60 (1), 59–68. https://doi.org/10.1016/j.addr.2007.06.011.
77. Figueiredo, L.; Cole, P. D.; Drachtman, R. A. Asparaginase Erwinia Chrysanthemi as a Component of a Multi-Agent Chemotherapeutic Regimen for the Treatment of Patients with Acute Lymphoblastic Leukemia Who Have Developed Hypersensitivity to E. Coli-Derived Asparaginase. *Expert Rev. Hematol.* **2016**, 9 (3), 227–234. https://doi.org/10.1586/17474086.2016.1142370.
78. Qi, Y.; Simakova, A.; Ganson, N. J.; Li, X.; Luginbuhl, K. M.; Ozer, I.; Liu, W.; Hershfield, M. S.; Matyjaszewski, K.; Chilkoti, A. A Brush-Polymer/Exendin-4 Conjugate Reduces Blood Glucose Levels for up to Five Days and Eliminates Poly(Ethylene Glycol) Antigenicity. *Nat. Biomed. Eng.* **2016**, 1 (1), 1–12. https://doi.org/10.1038/s41551-016-0002.
79. Qi, Y.; Chilkoti, A. Growing Polymers from Peptides and Proteins: A Biomedical Perspective. *Polym. Chem.* **2014**, 5 (2), 266–276. https://doi.org/10.1039/C3PY01089A.
80. Bai, S.; Ma, X.; Shi, X.; Shao, J.; Zhang, T.; Wang, Y.; Cheng, Y.; Xue, P.; Kang, Y.; Xu, Z. Smart Unimolecular Micelle-Based Polyprodrug with Dual-Redox Stimuli Response for Tumor Microenvironment: Enhanced in Vivo Delivery Efficiency and Tumor Penetration. *ACS Appl. Mater. Interfaces* **2019**. https://doi.org/10.1021/acsami.9b13214.
81. Ozer, I.; Tomak, A.; Zareie, H. M.; Baran, Y.; Bulmus, V. Effect of Molecular Architecture on Cell Interactions and Stealth Properties of PEG. *Biomacromolecules* **2017**, 18 (9), 2699–2710. https://doi.org/10.1021/acs.biomac.7b00443.
82. Tasaki, K. Poly(Oxyethylene)−Water Interactions: A Molecular Dynamics Study. *J. Am. Chem. Soc.* **1996**, 118 (35), 8459–8469. https://doi.org/10.1021/ja951005c.
83. Smith, G. D.; Bedrov, D.; Borodin, O. Conformations and Chain Dimensions of Poly(Ethylene Oxide) in Aqueous Solution: A Molecular Dynamics Simulation Study. *J. Am. Chem. Soc.* **2000**, 122 (39), 9548–9549. https://doi.org/10.1021/ja001053j.
84. Smith, G. D.; Bedrov, D.; Borodin, O. Molecular Dynamics Simulation Study of Hydrogen Bonding in Aqueous Poly(Ethylene Oxide) Solutions. *Phys. Rev. Lett.* **2000**, 85 (26), 5583–5586. https://doi.org/10.1103/PhysRevLett.85.5583.
85. Lee, H.; de Vries, A. H.; Marrink, S.-J.; Pastor, R. W. A Coarse-Grained Model for Polyethylene Oxide and Polyethylene Glycol: Conformation and Hydrodynamics. *J. Phys. Chem. B* **2009**, 113 (40), 13186–13194. https://doi.org/10.1021/jp9058966.
86. Lee, H.; Venable, R. M.; Alexander D MacKerell, J.; Pastor, R. W. Molecular Dynamics Studies of Polyethylene Oxide and Polyethylene Glycol: Hydrodynamic Radius and Shape Anisotropy. *Biophys. J.* **2008**, 95 (4), 1590. https://doi.org/10.1529/biophysj.108.133025.
87. Oelmeier, S. A.; Dismer, F.; Hubbuch, J. Molecular Dynamics Simulations on Aqueous Two-Phase Systems - Single PEG-Molecules in Solution. *BMC Biophys.* **2012**, 5, 14. https://doi.org/10.1186/2046-1682-5-14.
88. Kaiser, A.; Ismailova, O.; Koskela, A.; Huber, S. E.; Ritter, M.; Cosenza, B.; Benger, W.; Nazmutdinov, R.; Probst, M. Ethylene Glycol Revisited: Molecular Dynamics Simulations and Visualization of the Liquid and Its Hydrogen-Bond Network. *J. Mol. Liq.* **2014**, 189 (100), 20–29. https://doi.org/10.1016/j.molliq.2013.05.033.

89. Hoffmann, M. M.; Too, M. D.; Paddock, N. A.; Horstmann, R.; Kloth, S.; Vogel, M.; Buntkowsky, G. Molecular Dynamics Study of the Green Solvent Polyethylene Glycol with Water Impurities. *Molecules* **2024**, 29 (9), 2070. https://doi.org/10.3390/molecules29092070.
90. Gao, W.; Liu, W.; Christensen, T.; Zalutsky, M. R.; Chilkoti, A. In Situ Growth of a PEG-like Polymer from the C Terminus of an Intein Fusion Protein Improves Pharmacokinetics and Tumor Accumulation. *Proc. Natl. Acad. Sci.* **2010**, 107 (38), 16432–16437. https://doi.org/10.1073/pnas.1006044107.
91. Cheng, G.; Melnichenko, Y. B.; Wignall, G. D.; Hua, F.; Hong, K.; Mays, J. W. Small Angle Neutron Scattering Study of Conformation of Oligo(Ethylene Glycol)-Grafted Polystyrene in Dilute Solutions: Effect of the Backbone Length. *Macromolecules* **2008**, 41 (24), 9831–9836. https://doi.org/10.1021/ma801370q.
92. Johnson, E. C.; Murdoch, T. J.; Gresham, I. J.; Humphreys, B. A.; Prescott, S. W.; Nelson, A.; Webber, G. B.; Wanless, E. J. Temperature Dependent Specific Ion Effects in Mixed Salt Environments on a Thermoresponsive Poly(Oligoethylene Glycol Methacrylate) Brush. *Phys. Chem. Chem. Phys.* **2019**, 21 (8), 4650–4662. https://doi.org/10.1039/C8CP06644B.
93. Dalgakiran, E.; Tatlipinar, H. A Computational Study on the LCST Phase Transition of a POEGMA Type Thermoresponsive Block Copolymer: Effect of Water Ordering and Individual Behavior of Blocks. *J. Phys. Chem. B* **2019**, 123 (6), 1283–1293. https://doi.org/10.1021/acs.jpcb.8b11775.
94. Aitken, H. M.; Jiang, Z.; Hampton, I.; O'Mara, M. L.; Connal, L. A. Polymer–Solvent Interactions as a Tool to Engineer Material Properties. *Mol. Syst. Des. Eng.* **2022**, 7 (7), 746–754. https://doi.org/10.1039/D1ME00111F.
95. Choi, Y. K.; Park, S.-J.; Park, S.; Kim, S.; Kern, N. R.; Lee, J.; Im, W. CHARMM-GUI Polymer Builder for Modeling and Simulation of Synthetic Polymers. *J. Chem. Theory Comput.* **2021**, 17 (4), 2431–2443. https://doi.org/10.1021/acs.jctc.1c00169.
96. Team, T. A. Avogadro - Free cross-platform molecular editor. *Avogadro*, **2022**. https://avogadro.cc/ (accessed 2024-12-23).
97. Boyle, N. M.; James, A.; Morely C. ; Open babel: An open chemical toolbox. *Journal of Cheminformatics*. **2011**, 3(1). doi:10.1186/1758-2946-3-33.
98. SilcsBio. *CGENFF*. CGENFF. https://cgenff.com/ (accessed **2024**-10-23).
99. Jorgensen, W. L.; Chandrasekhar, J.; Madura, J. D.; Impey, R. W.; Klein, M. L. Comparison of Simple Potential Functions for Simulating Liquid Water. *J. Chem. Phys.* **1983**, 79 (2), 926–935. https://doi.org/10.1063/1.445869.
100. Price, D. J.; Brooks, C. L., III. A Modified TIP3P Water Potential for Simulation with Ewald Summation. *J. Chem. Phys*. **2004**, 121 (20), 10096–10103. https://doi.org/10.1063/1.1808117.
101. Plimpton, S. J.; Kohlmeyer, A.; Thompson, A. P.; Moore, S. G.; Berger, R. LAMMPS: Large-Scale Atomic/Molecular Massively Parallel Simulator, **2023**. https://doi.org/10.5281/ZENODO.10806852.
102. Nosé, S. A Unified Formulation of the Constant Temperature Molecular Dynamics Methods. *J. Chem. Phys*. **1984**, 81 (1), 511–519. https://doi.org/10.1063/1.447334.
103. Hoover, W. G. Canonical Dynamics: Equilibrium Phase-Space Distributions. *Phys. Rev. A* **1985**, 31 (3), 1695–1697. https://doi.org/10.1103/PhysRevA.31.1695.
104. Thompson, A. P.; Aktulga, H. M.; Berger, R.; Bolintineanu, D. S.; Brown, W. M.; Crozier, P. S.; In 'T Veld, P. J.; Kohlmeyer, A.; Moore, S. G.; Nguyen, T. D.; Shan, R.; Stevens, M. J.; Tranchida, J.; Trott, C.; Plimpton, S. J. LAMMPS - a Flexible Simulation Tool for Particle-Based Materials Modeling at the Atomic, Meso, and Continuum Scales. *Comput. Phys. Commun.* **2022**, 271, 108171. https://doi.org/10.1016/j.cpc.2021.108171.

105. Lee, J.; Cheng, X.; Jo, S.; MacKerell, A. D.; Klauda, J. B.; Im, W. CHARMM-GUI Polymer Builder for Modeling and Simulation of Synthetic Polymers | *Journal of Chemical Theory and Computation.* **2021**, 17 (5), 2431–2443. https://doi.org/10.1021/acs.jctc.1c00169.
106. Spivak, M.; Stone, J. E.; Ribeiro, J.; Saam, J.; Freddolino, L.; Bernardi, R. C.; Tajkhorshid, E. VMD as a Platform for Interactive Small Molecule Preparation and Visualization in Quantum and Classical Simulations. *J. Chem. Inf. Model.* **2023**, 63 (15), 4664–4678. https://doi.org/10.1021/acs.jcim.3c00658.
107. Gowers, R.; Linke, M.; Barnoud, J.; Reddy, T.; Melo, M.; Seyler, S.; Domański, J.; Dotson, D.; Buchoux, S.; Kenney, I.; Beckstein, O. MDAnalysis: A Python Package for the Rapid Analysis of Molecular Dynamics Simulations; *Austin, Texas,* **2016**; pp 98–105. https://doi.org/10.25080/Majora-629e541a-00e.
108. Bisong, E. Google Colaboratory. In Building Machine Learning and Deep Learning Models on Google Cloud Platform: A Comprehensive Guide for Beginners; *Bisong, E., Ed.; Apress: Berkeley, CA,* **2019**; pp 59–64. https://doi.org/10.1007/978-1-4842-4470-8_7.
109. Graphing and Data Analysis for Mac and Windows - *KaleidaGraph version 4.5.4 for Windows, Synergy Software*. **2024**, https://www.synergy.com/.
110. Guo, F.; Zhang, H.; Hu, H.-Q.; Cheng, X.-L. Effects of Hydrogen Bonds on Solid State TATB, RDX, and DATB under High Pressures. *Chin. Phys. B* **2014**, 23 (4), 046501. https://doi.org/10.1088/1674-1056/23/4/046501.
111. TRUBA HPC -*ULAKBIM/TÜBİTAK, Ankara, Türkiye*, **2021**, https://www.ulakbim.gov.tr.

Appendix A.

GRAPHS OF RADIUS OF GYRATION ANALYSIS

RADIUS OF GYRATION ANALYSIS, TCL script

```
# Define the polymer selection based on atom names or types
set molid [molinfo top]    ; # Get the molecule ID
set polymer_sel [atomselect $molid "name or type of polymer atoms"]
# Open a file to save the radius of gyration for each frame
set output_file [open "radius_of_gyrationeq.dat" w]
puts $output_file " # Frame Radius_of_Gyration (Å)"
# Loop over all frames in the trajectory
set nframes [molinfo $molid get numframes]
for {set i 0} {$i < $nframes} {incr i} {
    # Update the selection to the current frame
    $polymer_sel frame $i
    $polymer_sel update
    # Calculate the radius of gyration
    set Rg [measure rgyr $polymer_sel]  ; # Get the radius of gyration
    # Check if Rg is valid
    if {$Rg != ""} {
        # Save the frame and radius of gyration to the output file
        puts $output_file "$i $Rg"
    } else {
        puts "Warning: Invalid selection or error in calculating Rg at frame $i."} }
# Close the output file
close $output_file
```

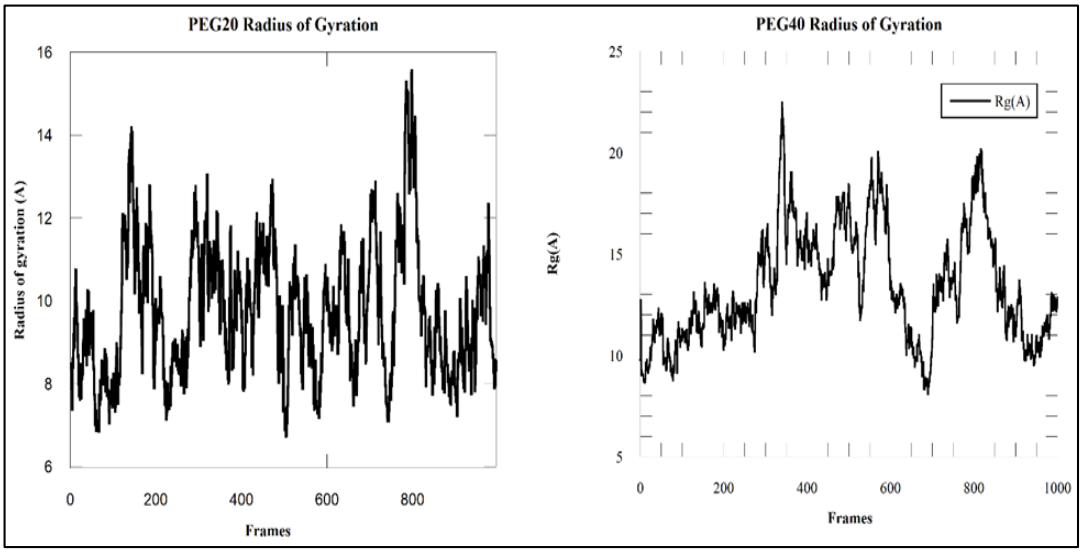

Figure A.1 PEG20(left) and PEG40(Right) radius of gyration

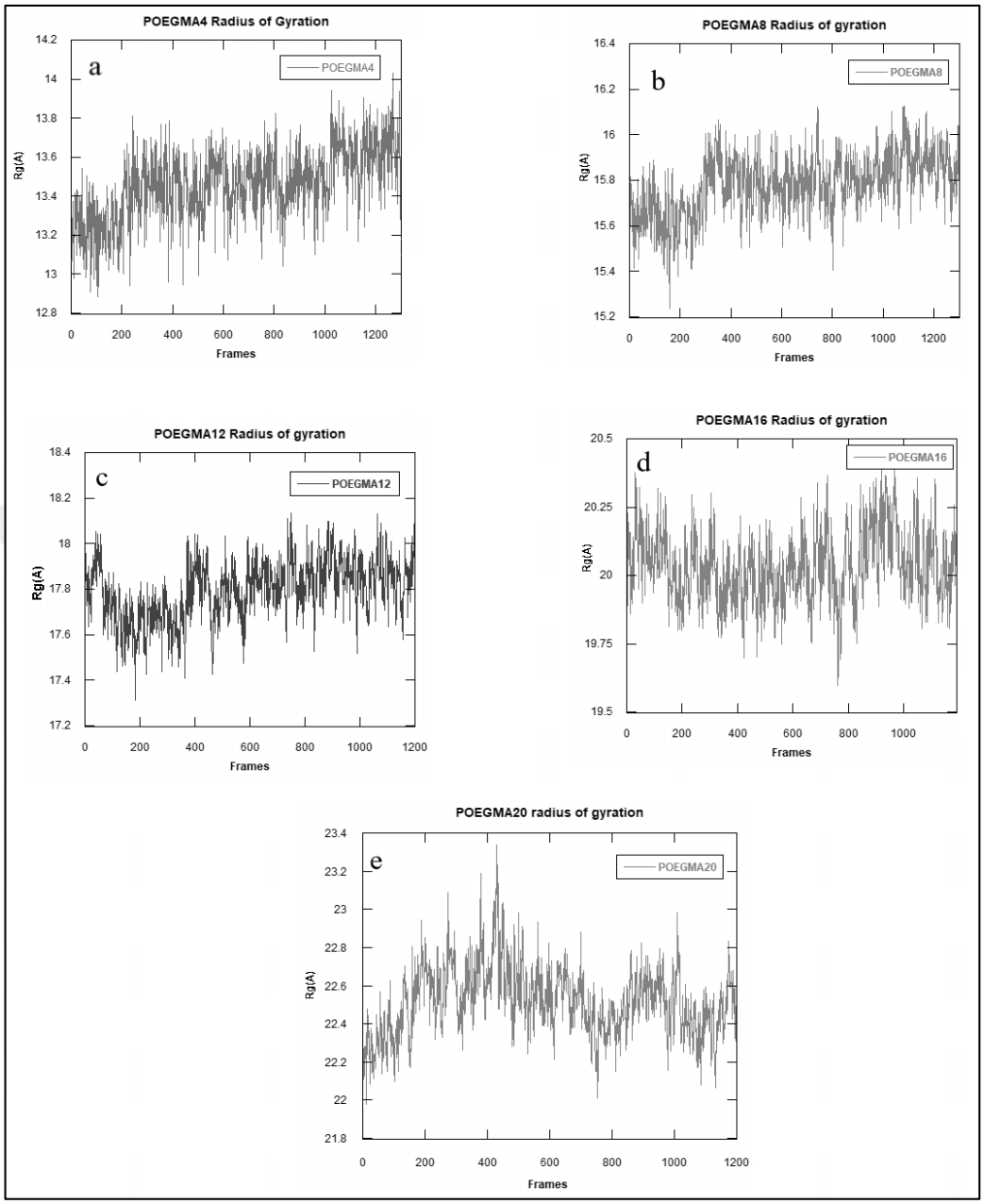

Figure A.2 All POEGMA Rg distribution plot

Appendix B.

GRAPHS OF WATERSHELL ANALYSIS

Watershell Analysis TCL Script

```
# Set the cutoff distance for considering water molecules around the polymer
set cutoff 5.0
# Define the polymer and water atom types
   set polymer_atoms [atomselect top "type polymer atom types"]
   set water_atoms [atomselect top "type water atom types"]
# Write output file
set output_file [open "wshellpeg20.dat" w]
# Get the total number of frames in the trajectory
set num_frames [molinfo top get numframes]
# Loop over all frames in the trajectory
for {set frame 0} {$frame < $num_frames} {incr frame} {
   # Update the frame
   animate goto $frame
   # Find water molecules within the cutoff distance of the polymer
   set water_within_cutoff [atomselect top "type $water_types and within $cutoff of type
$polymer_types"]
   # Count the number of unique water molecules within the cutoff distance
   set num_water [llength [lsort -unique [$water_within_cutoff get residue]]]
   # Print the results for the current frame
   puts $output_file "$frame $num_water"
 # Clean up selections
   $polymer_atoms delete
   $water_atoms delete
   $water_within_cutoff delete
}
# Close the output file
close $output_file
```

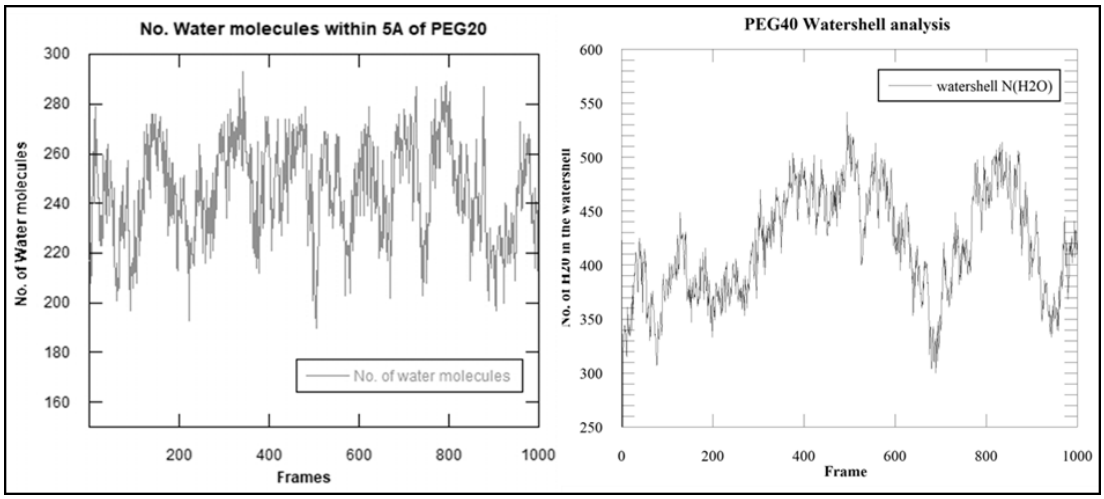

Figure B.1 PEG20(left) and PEG40(right) watershell N(H2O) plot for each frame

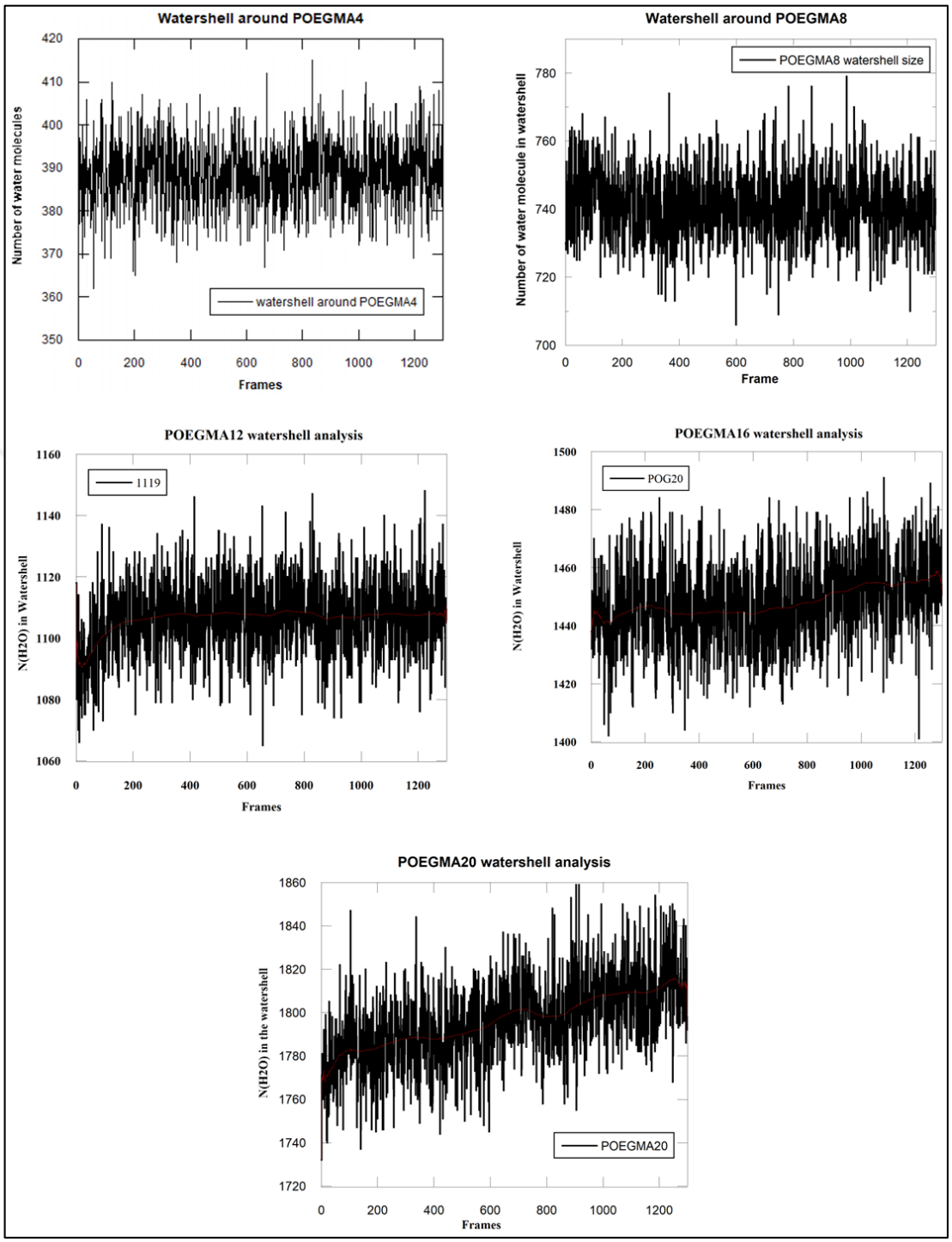

Figure B.2 POEGMA -4, -8, -12, -16 and -20mers watershell N(H2O)

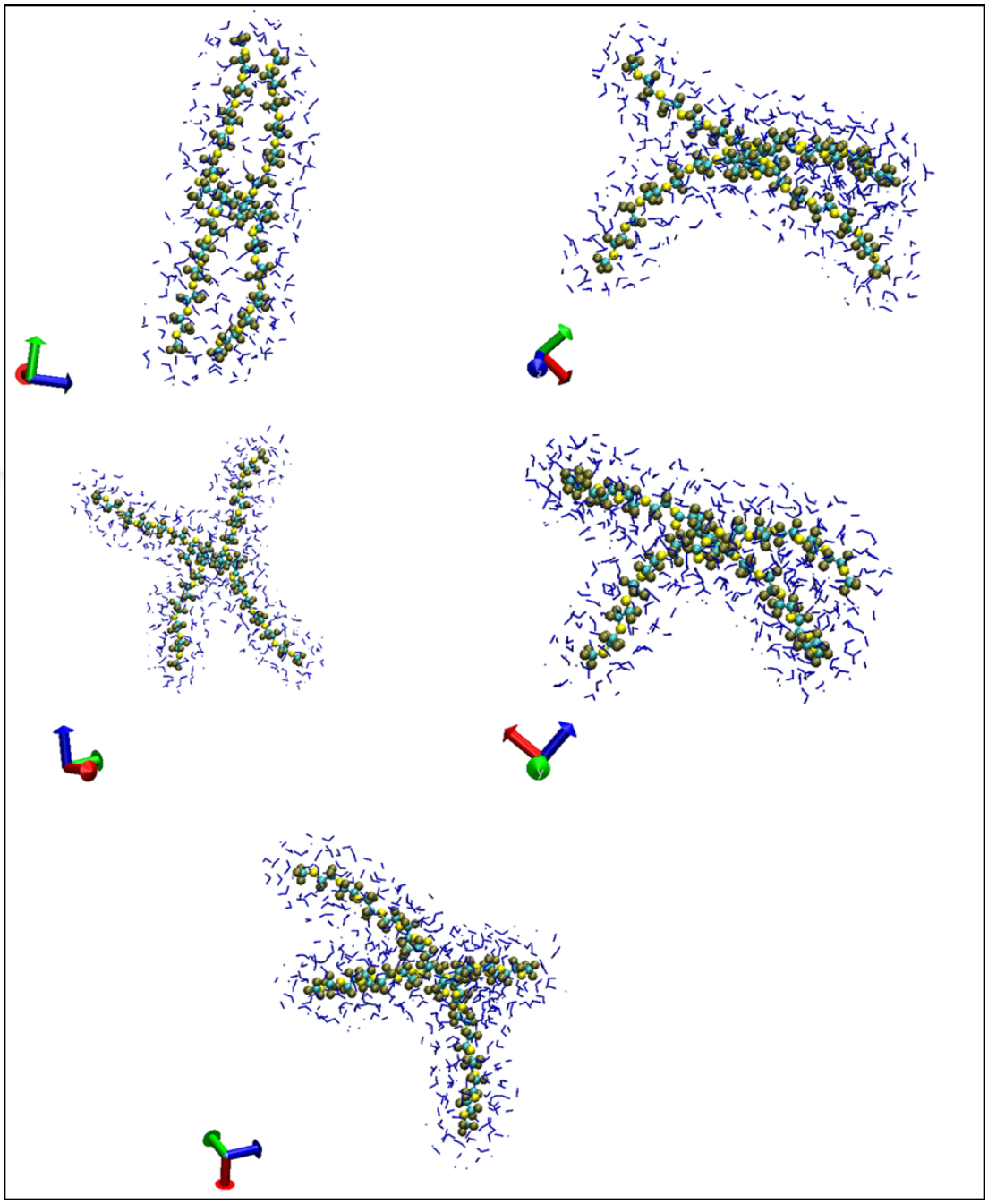

Figure B.3 POEGMA-4 snapshots at different stages of simulation run

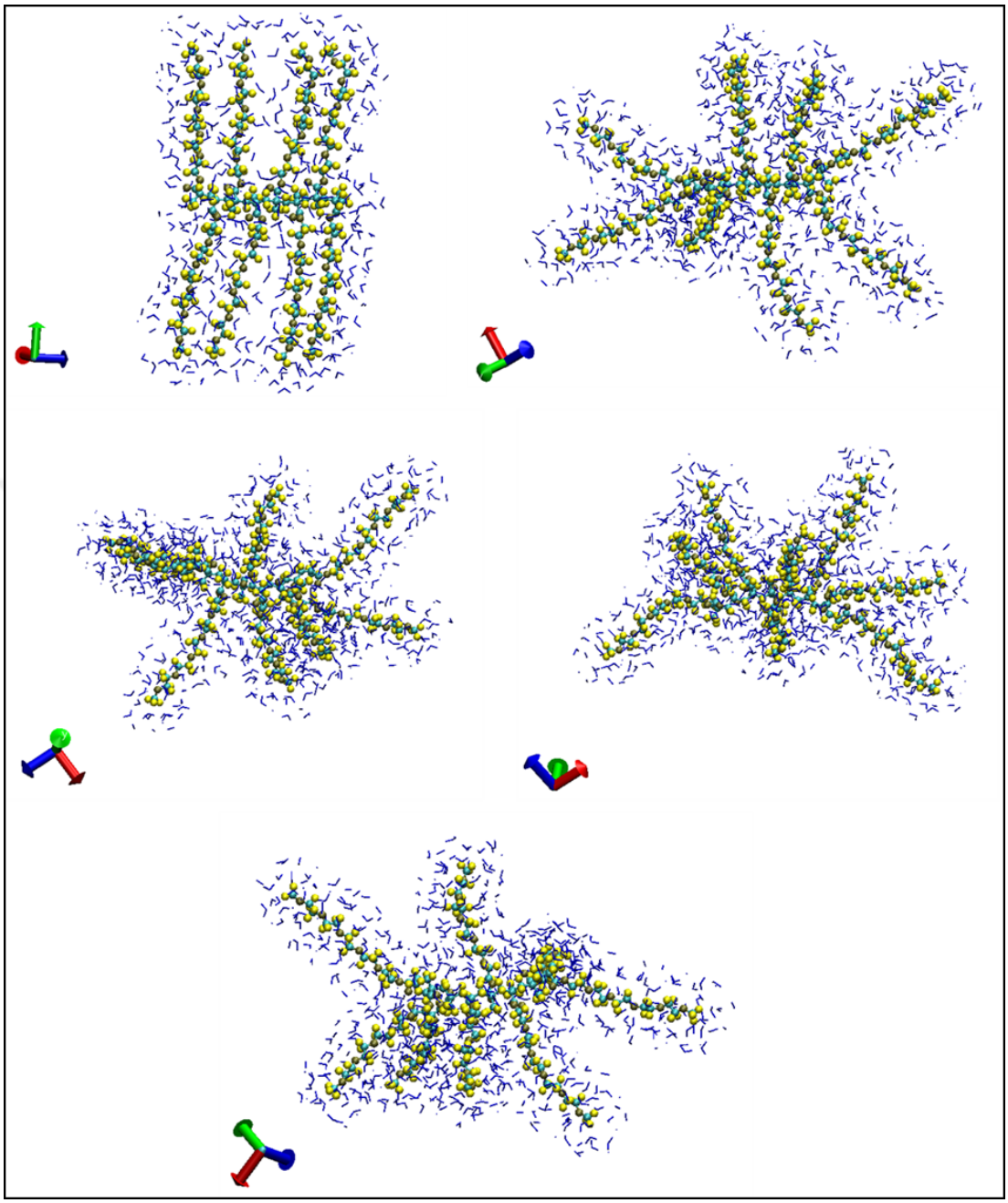

Figure B.4 POEGMA-8 Snapshots at different stages of simulation run

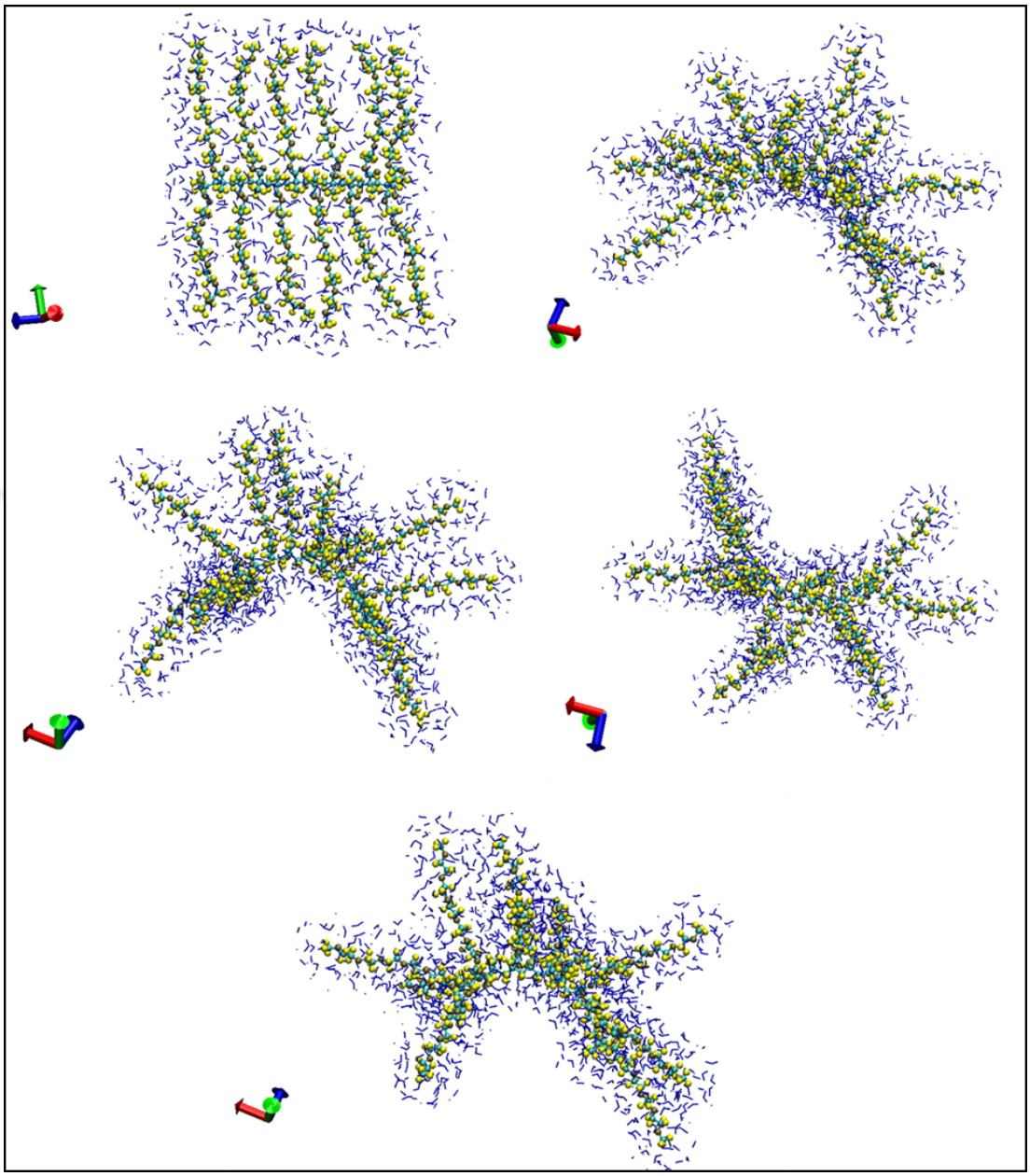

Figure B.5 POEGMA-12 snapshots at different stages of simulation run

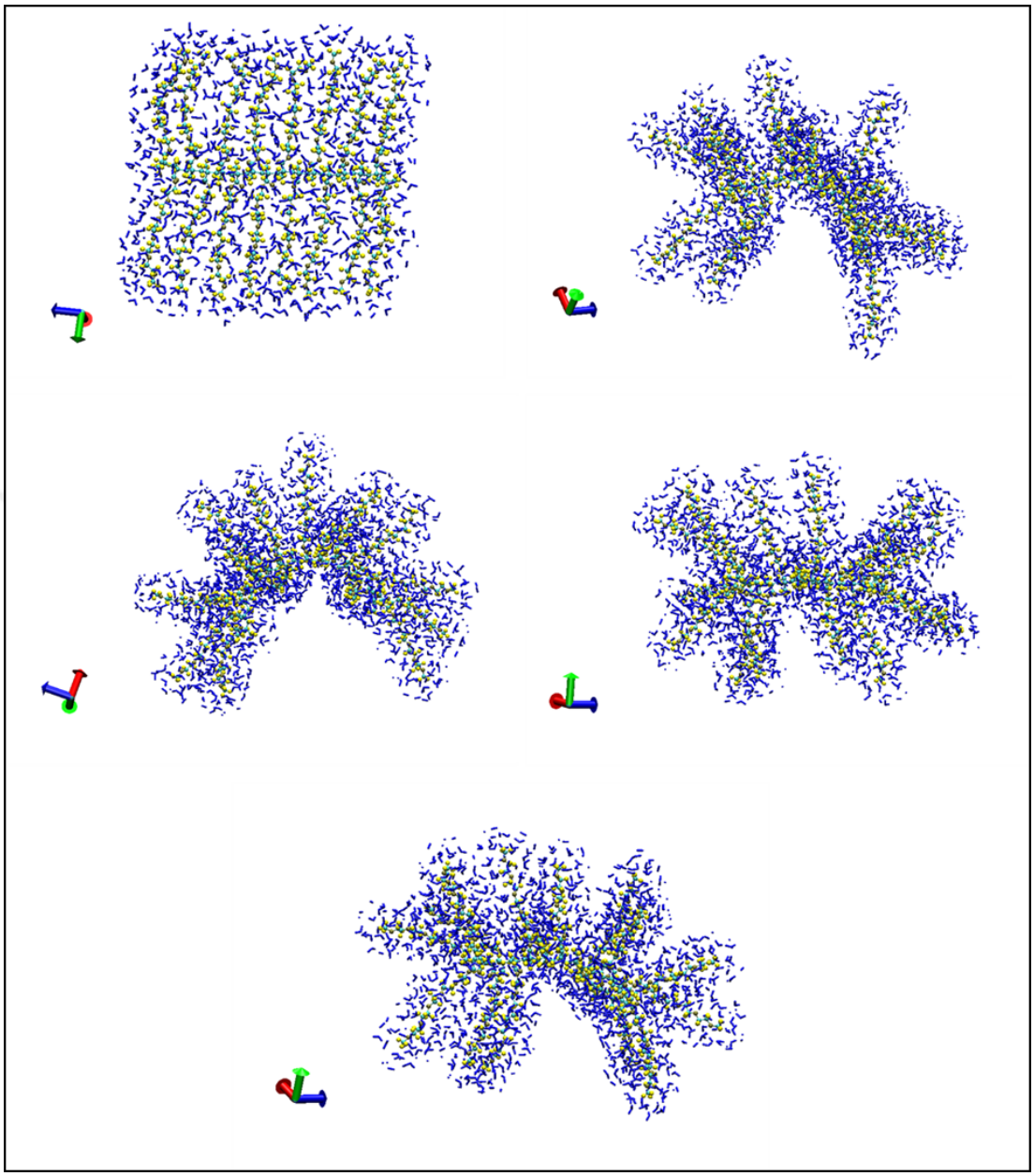

Figure B.6 POEGMA-16 Snapshots at different stages of simulation run

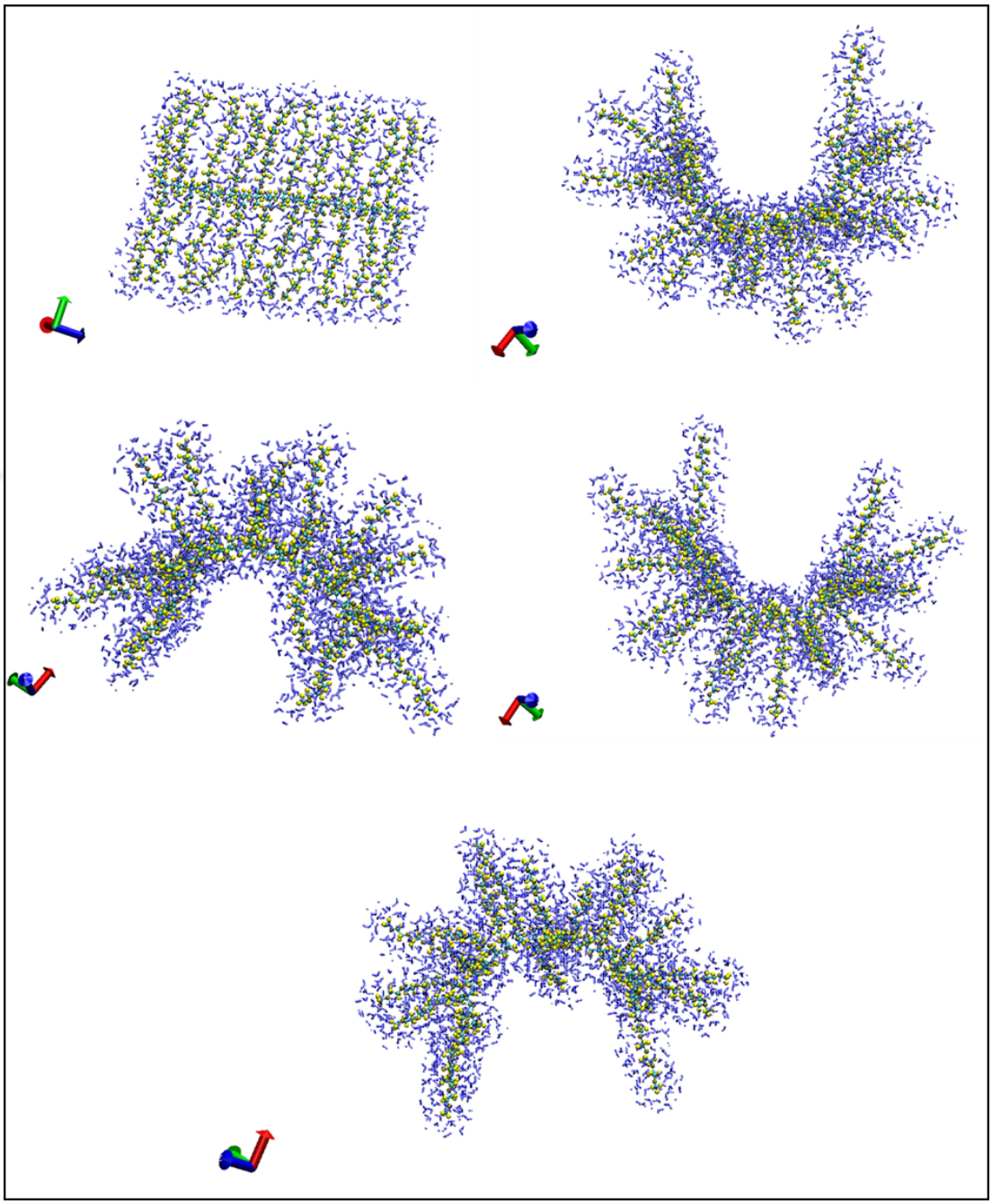

Figure B.7 POEGMA-20 snapshots at different stages of simulation run

Appendix C.

GRAPHS OF HYDROGEN BOND ANALYSIS

PYTHON script to calculate H-bond count using MDAnalysis

```
!pip install mdanalysis
import MDAnalysis
from MDAnalysis.analysis.hydrogenbonds.Hbond_analysis import
HydrogenBondAnalysis as HBA
H-bonds = HBA(u, hydrogens_sel=" water hydrogen atom type ",
        acceptors_sel=" Polymer Oxygen atom types", d_a_cutoff=3.5,
        d_h_a_angle_cutoff=135.0)
results = hbonds.run()
hbondinfo=results.hbonds
hbondinfo.shape
frames=hbondinfo[:,0]
donors=hbondinfo[:,1]
hydrogens=hbondinfo[:,2]
acceptors=hbondinfo[:,3]
#prints out the frameID, donor, hydrogen and acceptor information for each frame and
pair (real numbers, not zero-based).
for i in range(frames.shape[0]):
print(frames[i]+1,donors[i]+1,hydrogens[i]+1,acceptors[i]+1,distances[i],angles[i)
import csv
with open('hbpeg20.csv', 'w', newline='') as csvfile: # to Open file write mode ('w')
  writer = csv.writer(csvfile) # Create a CSV writer object
  writer.writerow(['Frame', 'Donor', 'Hydrogen', 'Acceptor', 'Distance', 'Angle'])
  # Iterate through the data and write each row
  for i in range(frames.shape[0]):
   writer.writerow([frames[i]+1, donors[i]+1, hydrogens[i]+1, acceptors[i]+1,
distances[i], angles[i]])
print("Data saved to hbond_data_peg20.csv")
```

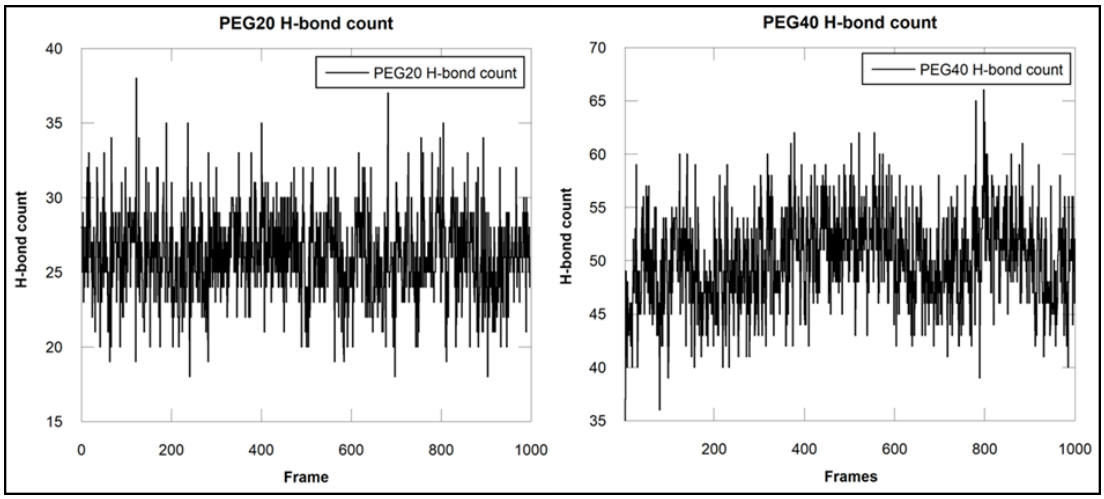

Figure C.1 PEG20 and PEG40 H-bond count distribution for each frame

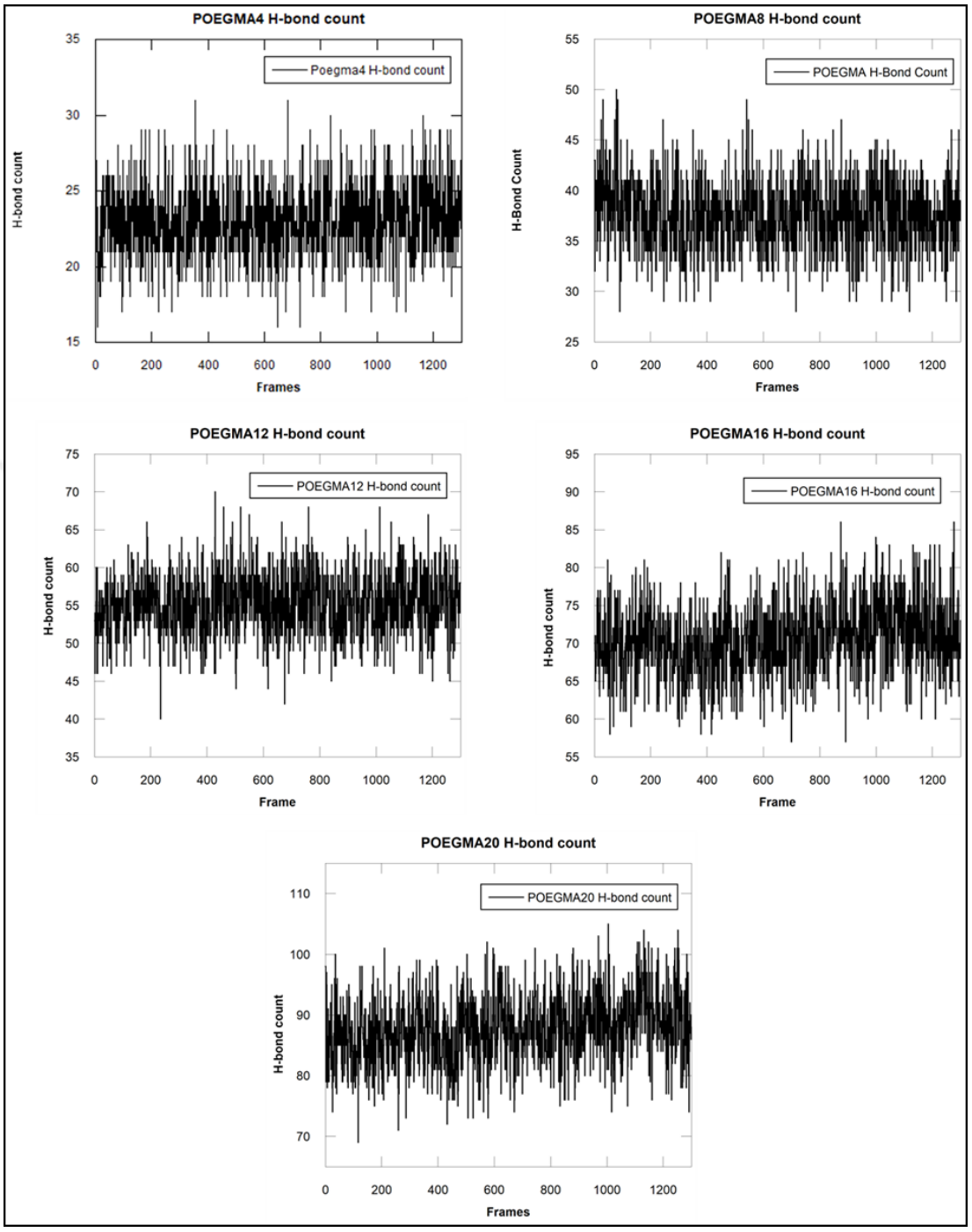

Figure C.2 POEGMA -4, -8, -12, -15 and -20mers H-bond count distribution